The Chaotic Obliquity of Mars

by

Jihad Rachid Touma

B.Sc., University of Texas at Austin (1988)

Submitted to the Department of Mathematics
in partial fulfillment of the requirements for the degree of

Doctor of Philosophy

at the

MASSACHUSETTS INSTITUTE OF TECHNOLOGY

September 1993

Author ..... Signature redacted
Department of Mathematics
August 16, 1993

Certified by ..... Signature redacted
Jack Wisdom
Professor of Planetary Science
Thesis Supervisor

Accepted by ..... Signature redacted
David Vogan
Chairman, Departmental Graduate Committee
Department of Mathematics

The Chaotic Obliquity of Mars

by

Jihad Rachid Touma

Submitted to the Department of Mathematics
on August 16, 1993, in partial fulfillment of the
requirements for the degree of
Doctor of Philosophy

Abstract

The n-body mapping method of Wisdom and Holman (1991) is generalized to encompass rotational dynamics. The Lie-Poisson structure of rigid body dynamics is discussed. Integrators which preserve that structure are derived for the motion of a free rigid body and for the motion of rigid bodies interacting gravitationally with mass points. Numerical integration of the rotation of Mars shows that the obliquity of Mars undergoes large chaotic variations. These variations occur as the system evolves in the chaotic zone associated with a secular spin-orbit resonance.

Thesis Supervisor: Jack Wisdom
Title: Professor of Planetary Science

Dedicated to the people of Southern Lebanon

Whose lives Israel shattered

While I was bringing these papers together.

Acknowledgments

On a scale of a lifetime, the story of how this work came to be, the story of my stay in the United States, is probably more important than the contents of these pages. It is tempting, therefore, to stretch the space of the acknowledgment and turn it into such a story. However, I will resist this temptation, as I resisted others during the writing of the dissertation, and express, succinctly, my deep gratitude to some of the people who made my adventure worth the effort.

I want to thank Victor Szebehely and Roger Broucke of the University of Texas at Austin for putting me on the path of celestial mechanics and Hamiltonian dynamics. This effort is a humble tribute to the excitement I remember feeling in courses and discussions I had with them.

Jack Wisdom, my thesis advisor, is a brilliant person to do science with, but most of all he is a sincere and humble mentor with whom it was always a pleasure to learn. I remember reading his papers in Texas and thinking "This is the kind of stuff I want to do". I did not know then that I would get to do it with as generous and supportive a friend as he was and I am sure will be.

Alar Toomre understood my limitations and helped me develop my strengths, and for that I am very grateful. It was most inspiring to see him capture in very simple pictures (literally pictures) seemingly complicated phenomena.

I thank Steven Strogatz and Gerald Sussman for their interest in my work and future, and for accepting to serve on my thesis committee.

My gratitude goes to Matt Holman with whom I tested most of the ideas I discuss here. I only hope that I can do the same for him (albeit longdistance) as he puts together his opus.

Phyllis Ruby made many a bureaucratic nightmare seem effortless. I am saddened to see her going through her current crisis with very little I can offer to help her feel better.

Aziz in Austin and Ranga in Cambridge are those rare friends with whom the social play of mirrors is constantly being challenged. Their social engagement and

tireless will to better the lives of beings around them offered me a sense of possibilities at times when my reading of circumstances didn't. I hope we will go on.

My friends at the Thistle and those in 2-342 were an essential part of my life at MIT. I single out Steve Penn, Esteban Tabak and Richard Eherenborg for the times we communicated when nothing else seemed to make sense.

My work owes a lot to my father Rachid, who in his home-grown work on distillation, blended experiment and theory in the best scientific tradition, and to my mother Laure, who managed to support my flight even when she found it difficult to understand my absence. My sister Nadine enriched our lives over the past four years and expanded our range of experience. It was rewarding to see her take off. I thank the other members of my family Walid, Catherine, Tanos, Manuella, Carolynn, Darwin, Kendall and Paige, for their support and advice.

My travel companion, Heather, enters at so many junctures into this story that it is futile to try to disentangle her role and present it in a coherent fashion. Together we have crossed boundaries, questioned norms, celebrated achievements and struggled through painful moments. In the months leading to my graduation, she was a tremendous source of support and "nourishment". As she gets ready to conclude her own research, I hope she finds my repertoire of Lebanese cuisine worth her investment.

Contents

List of Figures

List of Tables

Chapter 1

Introduction

There is a growing appreciation of the importance of understanding the dynamics of the solar system on very long timescales and there is no other way to study this dynamics other than long term numerical integration. Such long term computational journeys in the solar system are taking place with greater frequency. They have been made possible by improvements in computer hardware as well as improvements in numerical integration algorithms. As a recent example, Wisdom and Holman ([51], hereafter WH91) presented a new symplectic mapping method for integration of the planetary n- body problem which is an order of magnitude faster than conventional integrators. Sussman and Wisdom [36] used the new mapping method with the Supercomputer Toolkit (Abelson, et al. [1]), a specialized parallel supercomputer, to integrate the evolution of the whole solar system for 100 million years. That calculation confirmed the result of Laskar [24] that the evolution of the solar system is chaotic with an exponential divergence timescale of only 4-5 million years.

Rotational dynamics has so far not been considered in these adventures, though there is every reason to expect that important new discoveries are waiting to be made. In this work we extend the algorithmic developments of WH91 to encompass rigid body motion in the context of solar system dynamics. We introduce a symplectic scheme for integrating the motion of a free rigid body, which conserves the magnitude of the angular momentum vector and its orientation in space. Then, we incorporate gravitational interactions to obtain a symplectic scheme which integrates the motion

of rigid bodies interacting gravitationally with mass points, while preserving the total angular momentum vector. We use these algorithms to examine the rotational dynamics of Mars over one hundred million years. We find that the evolution is chaotic with an exponential divergence timescale of about 3-4 million years.

In chapter 2, we discuss the Lie-Poisson structure of rigid body dynamics and derive algorithms which integrate the motion of a free rigid body and of bodies interacting gravitationally with mass points. We study the stability of the free rigid body algorithm by examining the spurious resonances introduced by the discretization.

Chapter 3 is devoted to the study of the long-term rotational dynamics of Mars. We discuss the results of numerical integrations performed with the Lie-Poisson algorithms on an axisymmetric Mars interacting gravitationally with the solar system. We give evidence for the chaotic behavior of the rotation of Mars and link it to a secular spin-orbit resonance. We study a simple quasiperiodic model which captures the essential dynamics of the obliquity of Mars. We choose to focus on the physics and leave mathematical details to Appendix A.

We conclude in chapter 4 with a brief summary of our current knowledge about the history of planetary obliquities. We also outline certain directions that this work could/will take.

Chapter 2

Lie-Poisson Integrators for Rigid Body Dynamics in The Solar System

Our objective is to derive symplectic integrators for the motion of rigid bodies in the solar system. We require our integrators to conserve integrals of motion that result from the translational and rotational symmetries of the problems i.e. the total linear and angular momenta. We construct our symplectic integrators in the manner of WH91. We encode the Euclidean symmetries by moving to a relative coordinate system and by exploiting the Lie-Poisson formulation of rigid body dynamics. The story follows.

2.1 The Algorithm: Divide and Conquer

As described in WH91, symplectic mappings analogous to the n -body mapping method can be generated for any problem for which the Hamiltonian can be split into parts which are individually integrable and efficiently solvable. Consider a Hamiltonian of the form:

$$H = H_1 + H_2 \tag{2.1}$$

where H_1 and H_2 are individually efficiently solvable. The simplest mapping is obtained by multiplying the perturbation H_2 by a periodic sequence of Dirac delta functions:

$$H_{Map} = H_1 + 2\pi\delta_{2\pi}(\Omega t)H_2, \tag{2.2}$$

where

$$\delta_{2\pi}(t) = \sum_{n=-\infty}^{\infty} \delta(t - n2\pi) = \frac{1}{2\pi} \sum_{n=-\infty}^{\infty} \cos(nt), \tag{2.3}$$

and Ω is the mapping frequency, which is related to the stepsize h of the mapping by: $\Omega = 2\pi/h$. The motivation is the averaging principle: provided stepsize resonances are avoided (see [52] and below) the extra high frequency terms introduced by the delta functions tend to average out and do not substantially contribute to the evolution of the system. The advantage is that the evolution of the whole system can be computed in terms of the efficiently solvable pieces: between the delta functions the motion is entirely governed by H_1 and crossing the delta functions the evolution is governed solely by H_2. The simple mapping method, as just presented, is only accurate to first order in the stepsize, but has the correct average Hamiltonian. The mapping can be made accurate to second order while preserving the average Hamiltonian by offsetting the delta functions by half a mapping step. Higher order can be achieved by a more intricate interleaving of the evolutions governed by the integrable parts of the Hamiltonian. Of course, similar mappings can also be generated from Hamiltonians which are separated into more than two solvable parts, but achieving high order is more complicated, though perfectly straightforward. In what follows we concentrate on the efficient solution of parts of the Hamiltonian under the presumption that the method of putting them together to form the map of the desired order is understood.

Deriving a map for the problem of celestial rigid bodies appears to be a straightforward application of the procedure just described. We write the full Hamiltonian as a sum of integrable pieces:

$$H = H_{Euler} + H_{Kepler} + H_{Interaction}, \tag{2.4}$$

where H_{Euler} describes the free rigid body motion of each extended body, H_{Kepler} describes the interaction of each body with the massive central object (which may be

an extended body itself), and $H_{Interaction}$ includes all remaining gravitational interactions. Each of the components is separately integrable, as required. The problem with this direct application of the mapping procedure is that though the motion of the rigid body is integrable, to our knowledge, it is not efficiently solvable. The solution is complex and involves elliptic functions.

We can avoid the use of elliptic functions by further dividing the Hamiltonian for the free rigid body into two integrable pieces: a part which describes the integrable motion of an axisymmetric rigid body and an integrable perturbation which describes the triaxial deviation from axisymmetry. This division is motivated by the near axisymmetry of many bodies in the solar system; however, the algorithm is not limited to such situations. The solutions of these subproblems are simple and free of elliptic integrals.

This approach still has further problems. A fundamental problem in the description of the motion of the rigid body is that any choice of canonical angles, such as Euler angles, is singular. A complete covering of the phase space without singularities requires at least two independent coordinate systems (see, for example, [48]). So, we take Euler's advice and look at the motion of the angular momentum vector in a frame moving with the body. This move has the advantage of dealing with non-singular Cartesian components, and, for the free rigid body, of looking at the dynamics on the sphere defined by the conserved angular momentum. We first solve for the evolution of the Cartesian components of the angular momentum vector in the rigid body frame and then recover the configuration via a set of kinematic equations. Euler's equations have three dimensions; the phase space of the rigid body is six dimensional. Euler's approach to rigid body dynamics is a particular case of a more general formalism which can be used for reducing the dimensionality of problems with symmetry, the Lie-Poisson formalism. We make use of the Lie-Poisson formalism to derive singularity free algorithms for the problem at hand.

2.2 Gravitating Rigid Bodies

The Hamiltonian of a rigid body gravitationally interacting with a mass point is the sum of the kinetic and potential energy. The kinetic energy of a rigid body can be written as the sum of the translational kinetic energy of the center of mass and the kinetic energy of rotation about the center of mass. The potential energy is that of an arbitrary mass distribution in the Newtonian field of a mass point. The Hamiltonian is given by:

$$H = \frac{\vec{p}_1^2}{2m_1} + \frac{\vec{p}_2^2}{2m_2} + \frac{1}{2}\vec{M} \cdot \mathbf{I}^{-1}\vec{M} - \int_B \frac{Gm_1}{|\vec{r} + \mathbf{C}\vec{Q}|} dm(\vec{Q}), \tag{2.5}$$

where m_1, $\vec{r}_1$, and $\vec{p}_1$ are the mass, position, and linear momentum of the mass point S, and m_2, $\vec{r}_2$, and $\vec{p}_2$ are the mass, position of the center of mass, and the linear momentum of the rigid body B. The vector $\vec{r}$ is the relative position vector: $\vec{r} = \vec{r}_2 - \vec{r}_1$, and $dm(\vec{Q})$ is a differential mass element of the body at position $\vec{Q}$. The vector $\vec{M}$ is the angular momentum of B, and $\mathbf{I}$ is the inertia tensor. $\mathbf{C}$ is the orthogonal matrix that situates the body frame $\mathcal{B}$ with respect to the inertial frame $\mathcal{S}$. We denote by lowercase letters vectors in the inertial frame $\mathcal{S}$ and by upper case letters their counterparts in the rigid body frame $\mathcal{B}$. The generalization to more point masses or extended rigid bodies is straightforward and will be presented in later sections.

The Hamiltonian only depends on the relative positions of the bodies; a transformation to relative coordinates and center of mass coordinates separates the interesting relative dynamics from the trivial dynamics of the center of mass. The Hamiltonian for the relative motion is

$$H = \frac{\vec{p}^2}{2}\left(\frac{1}{m_1} + \frac{1}{m_2}\right) + \frac{1}{2}\vec{M} \cdot \mathbf{I}^{-1}\vec{M} - \int_B \frac{Gm_1}{|\vec{r} + \mathbf{C}\vec{Q}|} dm(\vec{Q}), \tag{2.6}$$

where $\vec{p}$ is the linear momentum conjugate to $\vec{r}$.

To derive the mapping we must separate the Hamiltonian into integrable pieces. We want to take advantage of the fact that the unperturbed motion consists of the composition of an elliptical two-body motion and of free rigid body motion governed by Euler's equations. With this in mind, we expand the potential function in terms of

Legendre polynomials. For the applications we have in mind, it is sufficient to consider the first three terms. Higher order terms can be included without a substantial increase in computational effort. This procedure gives us McCullagh's formula for the potential, which when incorporated with the kinetic energy yields the Hamiltonian :

$$H_2 = \underbrace{\frac{\vec{p}^2}{2}(\frac{1}{m_1}+\frac{1}{m_2}) + \frac{1}{2}\vec{M}\cdot\mathbf{I}^{-1}\vec{M} - \frac{Gm_1m_2}{r}}_{H_{Free}} \underbrace{- \frac{Gm_1}{2r^3}tr(\mathbf{I}) + \frac{3}{2}\frac{Gm_1}{r^5}\vec{R}\cdot\mathbf{I}\vec{R}}_{H_{Interaction}}. \quad (2.7)$$

In H_{Free}, the rotational and translational motions decouple. We write:

$$H_{Free} = H_{Kepler} + H_{Euler}, \quad (2.8)$$

where:

$$\begin{aligned} H_{Kepler} &= \frac{\vec{p}^2}{2}(\frac{1}{m_1}+\frac{1}{m_2}) - \frac{Gm_1m_2}{r} \\ H_{Euler} &= \frac{1}{2}\vec{M}\cdot\mathbf{I}^{-1}\vec{M}. \end{aligned} \quad (2.9)$$

We diagonalize $\mathbf{I}$ by choosing the principal axis frame as the body frame, and denote by I_1, I_2 and I_3 the moments of inertia about the principal axes oX, oY, and oZ, respectively. In the principal axis frame the rigid body Hamiltonian is

$$H_{Euler} = \frac{M_1^2}{2I_1} + \frac{M_2^2}{2I_2} + \frac{M_3^2}{2I_3}, \quad (2.10)$$

where M_1, M_2, and M_3 denote the components of the angular momentum on the principal axes.

As outlined earlier, we divide the rigid body Hamiltonian into two subHamiltonians:

$$H_{Euler} = \underbrace{\frac{M_1^2+M_2^2}{2I_2} + \frac{M_3^2}{2I_3}}_{H_{Axisymmetric}} + \underbrace{\frac{M_1^2}{2}(\frac{1}{I_1}-\frac{1}{I_2})}_{H_{Triaxial}}. \quad (2.11)$$

$H_{Axisymmetric}$ governs the motion of an axisymmetric body, and $H_{Triaxial}$ acts as a perturbation. This splitting is motivated by applications in solar system dynamics where departures from axisymmetry are often small, though the application of the mapping is not limited to problems with small triaxiality.

We must find efficiently computable solutions to each piece of the Hamiltonian. We first present a canonical version of the rigid body mapping, and then turn to the Lie-Poisson formalism.

2.3 Canonical Map for the Free Rigid Body

In this section the pieces of the free rigid body Hamiltonian are integrated in a convenient set of canonical coordinates, the Andoyer coordinates[2, 15]. The Andoyer momenta have simple physical interpretations in terms of the angular momentum and its projections in the body and inertial reference frames. In Andoyer variables the free rigid body Hamiltonian is cyclic in the coordinate conjugate to the total angular momentum; thus Andoyer variables naturally express the conservation of total angular momentum. This property is not shared by the traditional Euler angles. A further advantage of the Andoyer variables is that $H_{Axisymmetric}$ and $H_{Triaxial}$ are easily solved when expressed in terms of them.

Denote by $oxyz$ an inertial reference frame and by $oXYZ$ a frame rotating with the rigid body. Let $\vec{M}$ be the angular momentum vector as seen in the body frame, and Γ the plane normal to the angular momentum vector $\vec{M}$. The canonical system consists of the momenta:

- F, the projection of $\vec{M}$ on oz;
- G, the magnitude of $\vec{M}$;
- L, the projection of $\vec{M}$ on oZ,

and the angles conjugate to them:

- f, the angle between ox and the line of intersection of Γ with oxy.
- g, the angle between the lines of intersection of Γ with oxy and oXY;
- l, the angle between the line of intersection of Γ with oXY and oX;

From the definitions, it follows that:

$$\begin{aligned} M_1 &= \sqrt{G^2 - L^2}\,\sin(l), \\ M_2 &= \sqrt{G^2 - L^2}\,\cos(l), \\ M_3 &= L, \end{aligned} \tag{2.12}$$

where M_1, M_2 and M_3 are the components of $\vec{M}$ along oX, oY, and oZ, respectively. Using these we can reexpress the rigid body Hamiltonian in terms of the Andoyer variables:

$$H_{Euler} = \underbrace{\frac{G^2}{2I_2} + \frac{L^2}{2}(\frac{1}{I_3} - \frac{1}{I_2})}_{H_{Axisymmetric}} + \underbrace{\frac{(G^2 - L^2)\sin^2(l)}{2}(\frac{1}{I_1} - \frac{1}{I_2})}_{H_{Triaxial}}. \tag{2.13}$$

The equations of motion are derived via Hamilton's equations or equivalently the canonical Poisson bracket. We solve $H_{Axisymmetric}$ and $H_{Triaxial}$ separately, and then approximate the solutions of H_{Euler} with the method outlined above.

The Hamiltonian $H_{Axisymmetric}$ is cyclic in all the coordinates, so the momenta are conserved:

$$\begin{aligned} L(t) &= L(0), \\ l(t) &= L(0)(\frac{1}{I_3} - \frac{1}{I_2})\,t + l(0), \end{aligned} \tag{2.14}$$

and,

$$\begin{aligned} G(t) &= G(0), \\ g(t) &= \frac{G(0)}{I_2}\,t + g(0). \end{aligned} \tag{2.15}$$

Of course, F, which is a spatial component, is conserved, and with it the angle f.

The Hamiltonian $H_{Triaxial}$ is independent of F, and cyclic in g and f, so: $G(t) = G(0)$; $F(t) = F(0)$, and $f(t) = f(0)$. The other variables must satisfy:

$$\begin{aligned} \frac{d}{dt}l &= \frac{\partial}{\partial L}H_{Triaxial} = -\beta L\sin^2(l) \\ \frac{d}{dt}L &= -\frac{\partial}{\partial l}H_{Triaxial} = -\beta(G^2 - L^2)\sin(l)\cos(l) \\ \frac{d}{dt}g &= \frac{\partial}{\partial G}H_{Triaxial} = \beta G\sin^2(l), \end{aligned} \tag{2.16}$$

where $\beta = \frac{1}{I_1} - \frac{1}{I_2}$.

We can integrate these equations:

$$\begin{aligned} l(t) &= \arctan\left(\frac{M_1(0)}{M_2(0)\cos(\nu\,t) + M_3(0)\sin(\nu\,t)}\right) \\ L(t) &= -M_2(0)\sin(\nu\,t) + M_3(0)\cos(\nu\,t) \\ g(t) &= \arctan\left(\frac{M_3^2(0)\sin(\nu\,t) + M_1^2(0)\sin(\nu\,t) + M_2(0)\,M_3(0)\,\cos(\nu\,t)}{M_1(0)M(0)\cos(\nu\,t)}\right) \end{aligned} \tag{2.17}$$

where $M_1(0), M_2(0), M_3(0)$ and $M(0)$ are the initial values of the the angular momentum components and magnitude which we can compute in terms of $l(0), L(0)$ and $G(0)$, and $\nu = \beta M_1(0)$. These are the equations of a rotation about the X axis expressed in canonical coordinates.

Having solved for the flows generated by $H_{Axisymmetric}$ and $H_{Triaxial}$, we can use our method to construct approximations of the trajectories generated by H_{Euler} to the desired accuracy. Note that the transformations are symplectic and they explicitly conserve G and F.

2.4 Do the Right Thing: Euler's Move

A while ago, Euler demonstrated the simplicity of rigid body dynamics when seen in a frame that is rotating with the body. In the absence of external forces, the angular momentum vector is fixed in space, and the motion of the body can be recovered by following the projections of that vector on a basis fixed in the body.[4]

The configuration of the rigid body is specified by a special orthogonal transformation, $\mathbf{C} \in SO(3)$, which takes body vectors into space vectors:

$$\vec{v} = \mathbf{C}\vec{V}. \tag{2.18}$$

Since no torques are acting on the body, the angular momentum vector $\vec{m}$ is invariant in space:

$$\frac{d}{dt}\vec{m} = 0, \tag{2.19}$$

or,

$$\frac{d}{dt}(\mathbf{C}\vec{M}) = \mathbf{C}\frac{d}{dt}\vec{M} + (\frac{d}{dt}\mathbf{C})\vec{M} = 0. \tag{2.20}$$

For any time dependent orthogonal matrix $\mathbf{C}(t)$, $(\frac{d}{dt}\mathbf{C})\mathbf{C}^{-1}$ is skew symmetric, and, in the case of a rigid body, corresponds to the space angular velocity vector, $\vec{\omega}$:

$$(\frac{d}{dt}\mathbf{C})\mathbf{C}^{-1}\vec{v} = \vec{\omega} \times \vec{v}. \tag{2.21}$$

The body angular velocity vector is given by: $\vec{\Omega} = \mathbf{C}^{-1}\vec{\omega}$. Equation 2.20 reduces to:

$$\frac{d}{dt}\vec{M} = \vec{M} \times \vec{\Omega}. \tag{2.22}$$

The angular momentum and velocity vectors are related by the symmetric moment of inertia tensor $\mathbf{I}$:

$$\vec{M} = \mathbf{I}\vec{\Omega}. \tag{2.23}$$

So, we can rewrite Eq. (2.22):

$$\frac{d}{dt}\vec{M} = \vec{M} \times \mathbf{I}^{-1}\vec{M}. \tag{2.24}$$

Euler's equations, as these equations are known, put us directly on the angular momentum sphere and are free of singularities.

To get the time evolution of $\mathcal{B}$ with respect to $\mathcal{S}$, we need to follow $\mathbf{C}(t)$. We can do it directly by solving for the configuration matrix:

$$\frac{d}{dt}\mathbf{C} = \mathbf{C}\mathbf{S}[\mathbf{I}^{-1}\vec{M}], \tag{2.25}$$

where we denote by $\mathbf{S}[\vec{V}]$ the skew symmetric matrix associated with $\vec{V}$:

$$\mathbf{S}[\vec{V}] = \begin{pmatrix} 0 & -V_3 & V_2 \\ V_3 & 0 & -V_1 \\ -V_2 & V_1 & 0 \end{pmatrix}. \tag{2.26}$$

Alternatively, one can take an indirect route and follow the motion of a spatially fixed vector in the body frame. We adopt the second course since it fits naturally in the problem we are considering. Let $\vec{r}$ be an arbitrary vector fixed in $\mathcal{S}$: $\vec{R} = \mathbf{C}^{-1}\vec{r}$. Since $\frac{d}{dt}\vec{r} = 0$, the motion of $\vec{R}$ is governed by:

$$\frac{d}{dt}\vec{R} = \vec{R} \times \vec{\Omega} = \vec{R} \times \mathbf{I}^{-1}\vec{M}. \tag{2.27}$$

Clearly at any time t, we have: $\vec{R}(t) = \mathbf{C}^{-1}(t)\vec{r} = \mathbf{C}^{-1}(t)\mathbf{C}(0)\vec{R}(0)$. So, by solving Eq. (2.27), we isolate $\mathbf{C}^{-1}(t)$, and recover the configuration matrix $\mathbf{C}(t)$ by transposition.

In summary, the motion of a rigid body is governed by the equations:

$$\begin{aligned} \frac{d}{dt}\vec{M} &= \vec{M} \times \mathbf{I}^{-1}\vec{M} \\ \frac{d}{dt}\vec{R} &= \vec{R} \times \mathbf{I}^{-1}\vec{M}. \end{aligned} \tag{2.28}$$

2.5 Lie-Poisson Dynamics

An interesting feature of Euler's equations is that the rate of change of the components of the angular momentum is expressible solely in terms of the components of the angular momentum. Even though the phase space of the rigid body is six dimensional, the dynamics governing the angular momentum is only three dimensional. Now, the rate of change of any component of the angular momentum can be written as a Poisson bracket of that component with the rigid body Hamiltonian. Euler's equations show that the resulting Poisson bracket can be written solely in terms of the angular momentum. It turns out that a more general property holds: the Poisson bracket of any two functions of the angular momentum can be written solely in terms of the angular momentum. This property was known to Sophus Lie, and was first discussed in modern terms by Arnold [3]. Here, we give a coordinate dependent proof of this interesting feature which we shall use later to connect functions defined on the angular momentum sphere to the dynamics they generate.

The Cartesian components of $\vec{M}$ were expressed as functions of the canonical Andoyer variables in Eqs. (2.12). The Poisson bracket of the components of the angular momentum with an arbitrary function of the angular momentum $F(\vec{M})$ is

$$\begin{aligned}
\{M_1, F(\vec{M})\} &= \frac{\partial}{\partial l}M_1 \frac{\partial}{\partial L}F(\vec{M}) - \frac{\partial}{\partial L}M_1\frac{\partial}{\partial l}F(\vec{M}) \\
\{M_2, F(\vec{M})\} &= \frac{\partial}{\partial l}M_2 \frac{\partial}{\partial L}F(\vec{M}) - \frac{\partial}{\partial L}M_2\frac{\partial}{\partial l}F(\vec{M}) \\
\{M_3, F(\vec{M})\} &= \frac{\partial}{\partial l}M_3 \frac{\partial}{\partial L}F(\vec{M}) - \frac{\partial}{\partial L}M_3\frac{\partial}{\partial l}F(\vec{M})
\end{aligned} \tag{2.29}$$

We carry out the computations explicitly for M_1 and derive the others by analogy. We have:

$$\begin{aligned}
\frac{\partial}{\partial l}F &= \vec{\nabla}_{\vec{M}}F \cdot \frac{\partial}{\partial l}\vec{M} \\
\frac{\partial}{\partial L}F &= \vec{\nabla}_{\vec{M}}F \cdot \frac{\partial}{\partial L}\vec{M},
\end{aligned} \tag{2.30}$$

where $\vec{\nabla}_{\vec{M}}$ refers to the gradient with respect to the components of $\vec{M}$. Using

Eqs. (2.12), we get:

$$\begin{aligned}\frac{\partial}{\partial l}\vec{M} &= \begin{pmatrix} M_2 \\ -M_1 \\ 0 \end{pmatrix} \\ \frac{\partial}{\partial L}\vec{M} &= \begin{pmatrix} -\frac{M_3 M_1}{M_1^2+M_2^2} \\ -\frac{M_3 M_2}{M_1^2+M_2^2} \\ 1 \end{pmatrix}. \end{aligned} \tag{2.31}$$

Replacing in the equation for M_1, we get :

$$\begin{aligned}\{M_1, F(\vec{M})\} = \; & M_2\left(-\tfrac{\partial F}{\partial M_1}\tfrac{M_3 M_1}{M_1^2+M_2^2} - \tfrac{\partial F}{\partial M_2}\tfrac{M_3 M_2}{M_1^2+M_2^2} + \tfrac{\partial F}{\partial M_3}\right) \\ & + \tfrac{M_3 M_1}{M_1^2+M_2^2}\left(M_2\tfrac{\partial}{\partial M_1}F - M_1\tfrac{\partial}{\partial M_2}F\right), \end{aligned} \tag{2.32}$$

which after reduction gives:

$$\{M_1, F(\vec{M})\} = M_2\frac{\partial F}{\partial M_3} - M_3\frac{\partial F}{\partial M_2}. \tag{2.33}$$

Similarly, we find that:

$$\begin{aligned}\{M_2, F(\vec{M})\} &= M_3\frac{\partial F}{\partial M_1} - M_1\frac{\partial F}{\partial M_3} \\ \{M_3, F(\vec{M})\} &= M_1\frac{\partial F}{\partial M_2} - M_2\frac{\partial F}{\partial M_1}. \end{aligned} \tag{2.34}$$

Thus, we are able to express the canonical Poisson bracket of $\vec{M}$ with any real valued function F of $\vec{M}$, in terms of $\vec{M}$ alone:

$$\{\vec{M}, F\} = \vec{M} \times \vec{\nabla}_{\vec{M}} F. \tag{2.35}$$

In particular, when F is equal to H_{Euler}, $\vec{\nabla}_{\vec{M}} F = \mathbf{I}^{-1}\vec{M}$ and

$$\frac{d}{dt}\vec{M} = \{\vec{M}, F(\vec{M})\} = \vec{M} \times \mathbf{I}^{-1}\vec{M}, \tag{2.36}$$

which is Euler's equation.

We can generalize this computation by finding the Poisson bracket of two arbitrary real valued functions F_1 and F_2 of $\vec{M}$. The time derivative of F_1 along the trajectories generated by F_2 is given by:

$$\frac{d}{dt}F_1 = \vec{\nabla}_{\vec{M}} F_1 \cdot \frac{d}{dt}\vec{M} = \vec{\nabla}_{\vec{M}} F_1 \cdot \left(\vec{M} \times \vec{\nabla}_{\vec{M}} F_2\right) = -\vec{M} \cdot \left(\vec{\nabla}_{\vec{M}} F_1 \times \vec{\nabla}_{\vec{M}} F_2\right). \tag{2.37}$$

Thus,

$$\{F_1, F_2\} = -\vec{M} \cdot \left(\vec{\nabla}_{\vec{M}} F_1 \times \vec{\nabla}_{\vec{M}} F_2\right). \tag{2.38}$$

We can recover the equation governing the motion of a spatially fixed vector in the body frame within this formalism. We start by generalizing the configuration equation (2.25) to the case of the flow generated by an arbitrary Hamiltonian $F(\vec{M})$. Using Eq. (2.35), we rewrite Eq. (2.20) as:

$$\mathbf{C}\left(\vec{M} \times \vec{\nabla}_{\vec{M}} F\right) + (\frac{d}{dt}\mathbf{C})\vec{M} = 0. \tag{2.39}$$

Using the fact that this equation holds for any $\vec{M}$, we find:

$$\frac{d}{dt}\mathbf{C} = \mathbf{C}\mathbf{S}[\vec{\nabla}_{\vec{M}} F]. \tag{2.40}$$

Next, we consider an arbitrary space fixed vector $\vec{r} = \mathbf{C}\vec{R}$. As before, we can write:

$$\mathbf{C}\frac{d}{dt}\vec{R} + (\frac{d}{dt}\mathbf{C})\vec{R} = 0. \tag{2.41}$$

Using Eq. (2.40), we obtain:

$$\frac{d}{dt}\vec{R} = -\mathbf{S}[\vec{\nabla}_{\vec{M}} F]\vec{R}. \tag{2.42}$$

Expanding the matrix multiplication, we get:

$$\frac{d}{dt}\vec{R} = \{\vec{R}, F(\vec{M})\} = \vec{R} \times \nabla_{\vec{M}} F. \tag{2.43}$$

As before, when $F(\vec{M})$ is equal to H_{Euler}, we get the expected equation for $\vec{R}$:

$$\frac{d}{dt}\vec{R} = \vec{R} \times \vec{\nabla}_{\vec{M}} H_{Euler} = \vec{R} \times \mathbf{I}^{-1}\vec{M}. \tag{2.44}$$

Note that for any Hamiltonian H, which only depends on $\vec{M}$, the equations of motion generated by the Poisson bracket conserves the magnitude of $\vec{R}$:

$$\vec{R} \cdot \frac{d}{dt}\vec{R} = \vec{R} \cdot (\vec{R} \times \vec{\nabla}_{\vec{M}} H) = 0. \tag{2.45}$$

The same is true for $\vec{M}$. So, for any such H, the motion of $\vec{M}$ and $\vec{R}$ consists of finite rotations.

The reduction procedure is not specific to the free rigid body problem. A reduction of the Poisson bracket from a high dimensional phase space to one of lower dimensions, is possible whenever a group of symmetries acts on the original phase space. In the case that the phase space is the cotangent bundle of a Lie group, and the symmetry group is the Lie group itself, the reduction procedure leads to what is known as the Lie-Poisson bracket. This is precisely the case of the free rigid body problem where the configuration space is the group of special orthogonal transformations and the dual Lie algebra can be identified with the angular momentum space. In the next section, we derive a Lie-Poisson bracket for the problem of a rigid body interacting gravitationally with a mass point, a problem which is invariant under the group of Euclidean motions.

2.5.1 Spin-Orbit Lie-Poisson Bracket

Hamiltonian (2.6), the spin-orbit Hamiltonian, admits the group of Euclidean motions as a group of symmetry. This translates into the conservation of the total linear and angular momenta. We used the conservation of linear momentum when we moved to the center of mass frame. In order to enforce the rotational symmetry, we move to $\mathcal{B}$. Denoting vectors in the body by capital letters as before, $\vec{R}$ is the relative vector in the rigid body frame, and $\vec{P}$ is the relative linear momentum in the body frame. The equations of motion, including the kinematic accelerations, are:

$$\begin{aligned}
\frac{d}{dt}\vec{P} &= \vec{P}\times\mathbf{I}^{-1}\vec{M} - \int_B \frac{Gm_1(\vec{R}+\vec{Q})}{|\vec{R}+\vec{Q}|^3}dm(\vec{Q}),\\
\frac{d}{dt}\vec{R} &= \vec{R}\times\mathbf{I}^{-1}\vec{M} + \vec{P}(\frac{1}{m_1}+\frac{1}{m_2}),\\
\frac{d}{dt}\vec{M} &= \vec{M}\times\mathbf{I}^{-1}\vec{M} + \int_B \frac{Gm_1(\vec{R}\times\vec{Q})}{|\vec{R}+\vec{Q}|^3}dm(\vec{Q}).
\end{aligned} \tag{2.46}$$

After our discussion of Euler's equations, the reader should not be surprised to find out that these equations can be derived via a Poisson bracket of the various dynamic variables with the Hamiltonian expressed in the body frame:

$$\hat{H} = \frac{\vec{P}^2}{2}(\frac{1}{m_1}+\frac{1}{m_2}) + \frac{1}{2}\vec{M}\cdot\mathbf{I}^{-1}\vec{M} - \int_B \frac{Gm_1}{|\vec{R}+\vec{Q}|}dm(\vec{Q}). \tag{2.47}$$

A formal derivation of the bracket, which uses the differential structure of the Lie group of Euclidean motions, is given in Wang, Krishnaprasad, and Maddocks (1991). Here, we derive the bracket in a manner analogous to our derivation of the Lie-Poisson bracket for the free rigid body. To give an idea of what is involved, we derive the equations of the angular momentum vector. As argued before, we can express the angular momentum vector in terms of canonical variables. The canonical equations governing the evolution of $\vec{M}$ are:

$$\frac{d}{dt}\vec{M} = \left\{\vec{M}, H\right\}, \tag{2.48}$$

where the bracket denotes the canonical Poisson bracket. Applying the chain rule, we expand the Poisson bracket:

$$\left\{\vec{M}, H\right\} = \left\{\vec{M}, \hat{H}\right\} = \vec{M} \times \vec{\nabla}_{\vec{M}}\hat{H} - \sum_{i=1}^{3}\left[\vec{\nabla}_{\vec{R}}\hat{H} \cdot \{\vec{R}, M_i\}\right]\vec{e}_i - \sum_{i=1}^{3}\left[\vec{\nabla}_{\vec{P}}\hat{H} \cdot \{\vec{P}, M_i\}\right]\vec{e}_i, \tag{2.49}$$

where $\vec{e}_1$, $\vec{e}_2$, and $\vec{e}_3$ are unit vectors along axes oX, oY and oZ respectively. The $\vec{M}$ dependence of $\hat{H}$ gives the term $\vec{M} \times \vec{\nabla}_{\vec{M}}\hat{H}$ as shown before. Using Eq. (2.43), we get:

$$\begin{aligned} \{\vec{R}, M_i\} &= \vec{R} \times \nabla_{\vec{M}} M_i = \vec{R} \times \vec{e}_i, \\ \{\vec{P}, M_i\} &= \vec{P} \times \nabla_{\vec{M}} M_i = \vec{P} \times \vec{e}_i, \ i = 1, 2, 3. \end{aligned} \tag{2.50}$$

Replacing in Eq. (2.49) we get:

$$\frac{d}{dt}\vec{M} = \left\{\vec{M}, \hat{H}\right\} = \vec{M} \times \vec{\nabla}_{\vec{M}}\hat{H} + \vec{R} \times \vec{\nabla}_{\vec{R}}\hat{H} + \vec{P} \times \vec{\nabla}_{\vec{P}}\hat{H}. \tag{2.51}$$

The canonical structure, in addition to the reduction calculations, gives us the remaining equations for $\vec{R}$ and $\vec{P}$ in terms of a Poisson bracket:

$$\begin{aligned} \frac{d}{dt}\vec{R} &= \vec{R} \times \vec{\nabla}_{\vec{M}}\hat{H} + \vec{\nabla}_{\vec{P}}\hat{H} \\ \frac{d}{dt}\vec{P} &= \vec{P} \times \vec{\nabla}_{\vec{M}}\hat{H} - \vec{\nabla}_{\vec{R}}\hat{H}. \end{aligned} \tag{2.52}$$

If $\hat{H}$ happens to be the spin orbit coupling Hamiltonian, expressed in the rigid body frame, we get the expected equations for the motion of $\vec{M}$, $\vec{R}$ and $\vec{P}$.

Note that for any $\hat{H}(\vec{R}, \vec{P}, \vec{M})$, these equations preserve the total spatial angular momentum :

$$\vec{m}_{Total} = \vec{m} + \vec{r} \times \vec{p}, \tag{2.53}$$

as can be seen by taking the time derivative of $\vec{m}_{Total}$ and replacing $\frac{d}{dt}\vec{M}$, $\frac{d}{dt}\vec{R}$, and $\frac{d}{dt}\vec{P}$ with the Poisson brackets just derived.

Finally, we derive the Poisson bracket of two real valued functions, F_1 and F_2 , of $\vec{M}, \vec{R}$, and $\vec{P}$:

$$\begin{aligned}
\{F_1, F_2\} &= \vec{\nabla}_{\vec{M}} F_1 \cdot \left\{\vec{M}, F_2\right\} + \vec{\nabla}_{\vec{R}} F_1 \cdot \left\{\vec{R}, F_2\right\} + \vec{\nabla}_{\vec{P}} F_1 \cdot \left\{\vec{P}, F_2\right\} \\
&= -\vec{M} \cdot \left[\vec{\nabla}_{\vec{M}} F_1 \times \vec{\nabla}_{\vec{M}} F_2\right] \\
&\quad + \vec{R} \cdot \left[\vec{\nabla}_{\vec{R}} F_2 \times \vec{\nabla}_{\vec{M}} F_1 - \vec{\nabla}_{\vec{R}} F_1 \times \vec{\nabla}_{\vec{M}} F_2\right] \\
&\quad + \vec{P} \cdot \left[\vec{\nabla}_{\vec{P}} F_2 \times \vec{\nabla}_{\vec{M}} F_1 - \vec{\nabla}_{\vec{P}} F_1 \times \vec{\nabla}_{\vec{M}} F_2\right] \\
&\quad + \vec{\nabla}_{\vec{R}} F_1 \cdot \vec{\nabla}_{\vec{P}} F_2 - \vec{\nabla}_{\vec{P}} F_1 \cdot \vec{\nabla}_{\vec{R}} F_2.
\end{aligned} \tag{2.54}$$

With this, we end our adventure on Poisson manifolds. We will use the bracket derived in this section in the rest of the paper.

2.6 A Lie-Poisson Mapping for a Free Rigid Body

We use the Lie-Poisson bracket to derive a scheme that integrates the motion of a free rigid body, while preserving the symplectic structure (Poisson bracket) and the magnitude of the angular momentum vector. The angular momentum vector is naturally fixed in space. First, we integrate the Hamiltonians that enter into the construction. Then, we put the integral curves together to approximate the actual motion.

2.6.1 Axisymmetric Body: Exact Solution

We solve for the motion of an axisymmetric body. Assume, for definiteness, that the body is symmetric about the Z axis, i.e. $I_1 = I_2 = I$. The Hamiltonian is given by:

$$H = \frac{M_1^2 + M_2^2}{2\,I} + \frac{M_3^2}{2\,I_3}. \tag{2.55}$$

Euler's equations become:

$$\begin{aligned} \frac{d}{dt}M_1 &= M_3 M_2(\frac{1}{I_3} - \frac{1}{I}) \\ \frac{d}{dt}M_2 &= -M_1 M_3(\frac{1}{I_3} - \frac{1}{I}) \\ \frac{d}{dt}M_3 &= 0. \end{aligned} \tag{2.56}$$

These equations govern the precession of the angular momentum vector around the axis of symmetry. Setting $\alpha = (\frac{1}{I_3} - \frac{1}{I})M_3(0)$, we integrate to get :

$$\vec{M}(t) = \begin{pmatrix} \cos(\alpha\, t) & \sin(\alpha\, t) & 0 \\ -\sin(\alpha\, t) & \cos(\alpha\, t) & 0 \\ 0 & 0 & 1 \end{pmatrix} \vec{M}(0) = \mathbf{C}_Z(\alpha\, t)\vec{M}(0). \tag{2.57}$$

Next, we solve for the motion of $\vec{R}$:

$$\frac{d}{dt}\vec{R} = \vec{R} \times \mathbf{I}^{-1}\vec{M}(t), \tag{2.58}$$

or, using Eq. (2.57) :

$$\frac{d}{dt}\vec{R} = \vec{R} \times \mathbf{I}^{-1}\mathbf{C}_Z(\alpha\, t)\vec{M}(0). \tag{2.59}$$

It is easy to check that, in the case we are considering, $\mathbf{I}^{-1}\mathbf{C}_Z = \mathbf{C}_Z\mathbf{I}^{-1}$. Next, transform to a frame that is precessing with $\vec{M}$:

$$\vec{R}(t) = \mathbf{C}_Z(\alpha\, t)\vec{R}_p(t). \tag{2.60}$$

Replacing in Eq. (2.59), we get :

$$(\frac{d}{dt}\mathbf{C}_Z)\vec{R}_p + \mathbf{C}_Z\frac{d}{dt}\vec{R}_p = \mathbf{C}_Z\vec{R}_p \times [\mathbf{C}_Z\mathbf{I}^{-1}\vec{M}(0)]. \tag{2.61}$$

Noting that $\mathbf{C}_Z a \times \mathbf{C}_Z b = \mathbf{C}_Z(a \times b)$, and that $\mathbf{C}_Z^{-1} = \mathbf{C}_Z^T$,we can rewrite Eq. (2.61):

$$\frac{d}{dt}\vec{R}_p = \vec{R}_p \times \mathbf{I}^{-1}\vec{M}(0) - \mathbf{C}_Z^T(\frac{d}{dt}\mathbf{C}_Z)\vec{R}_p. \tag{2.62}$$

But,

$$\mathbf{C}_Z^T\frac{d}{dt}\mathbf{C}_Z = \begin{pmatrix} 0 & \alpha & 0 \\ -\alpha & 0 & 0 \\ 0 & 0 & 0 \end{pmatrix}. \tag{2.63}$$

So, reducing the right-hand side of Eq. (2.62), we end up with:

$$\frac{d}{dt}\vec{R}_p = \begin{pmatrix} 0 & \frac{M_3(0)}{I} & -\frac{M_2(0)}{I} \\ -\frac{M_3(0)}{I} & 0 & \frac{M_1(0)}{I} \\ \frac{M_2(0)}{I} & -\frac{M_1(0)}{I} & 0 \end{pmatrix} \vec{R}_p = \vec{R}_p \times \frac{\vec{M}(0)}{I}. \tag{2.64}$$

These equations govern the precession of the vector $\vec{R}_p$ around the vector $\vec{\Omega}(0) = \vec{M}(0)/I$. The solution is given by the Euler-Rodrigues formula (see Goldstein, 1980):

$$\vec{R}_p(t) = \mathbf{C}_{\vec{\Omega}}(\beta t)\vec{R}_p(0), \tag{2.65}$$

where

$$\mathbf{C}_{\vec{\Omega}}(\beta t) = cos(\beta t)\,\mathbf{1} + \frac{\sin(\beta t)}{\beta}\,\mathbf{S}\left[\vec{\Omega}(0)\right] + \frac{1-\cos(\beta t)}{\beta^2}\,\mathbf{S}^2\left[\vec{\Omega}(0)\right], \tag{2.66}$$

where $\mathbf{1}$ is the identity matrix, $\beta = -|\vec{\Omega}(0)|$ and $\mathbf{S}[\vec{\Omega}(0)]$ is the skew symmetric matrix corresponding to $\vec{\Omega}(0)$. Thus, we obtain:

$$\vec{R}(t) = \left(\mathbf{C}_Z(\alpha t)\mathbf{C}_{\vec{\Omega}}(\beta t)\right)\vec{R}(0). \tag{2.67}$$

Finally, we update the configuration of the rigid body via:

$$\mathbf{C}(t) = \mathbf{C}(0)\left(\mathbf{C}_{\vec{\Omega}}^{-1}(\beta t)\mathbf{C}_Z^{-1}(\alpha t)\right). \tag{2.68}$$

2.6.2 Integrating the Triaxial Perturbation

The subHamiltonian $H_{Triaxial}$ is of the form:

$$H_{M_i} = \alpha_i \frac{M_i^2}{2}, i = 1, 2, 3. \tag{2.69}$$

We solve H_{M_1} in detail, and solve the others by analogy.

We compute the Poisson bracket using H_{M_1} . The angular momentum vector evolves according to:

$$\frac{d}{dt}\vec{M} = \vec{M} \times \vec{\nabla}_{\vec{M}} H_{M_1} = \vec{M} \times \begin{pmatrix} \alpha_1 M_1 \\ 0 \\ 0 \end{pmatrix}, \tag{2.70}$$

or

$$\frac{d}{dt}\begin{pmatrix} M_1 \\ M_2 \\ M_3 \end{pmatrix} = \begin{pmatrix} 0 \\ \alpha_1 M_1 M_3 \\ -\alpha_1 M_1 M_2 \end{pmatrix}. \tag{2.71}$$

These equations govern a rotation about the X axis with frequency $\alpha_1 M_1(0)$:

$$\vec{M}(t) = \begin{pmatrix} 1 & 0 & 0 \\ 0 & \cos(\alpha_1 M_1(0)\, t) & \sin(\alpha_1 M_1(0)\, t) \\ 0 & -\sin(\alpha_1 M_1(0)\, t) & \cos(\alpha_1 M_1(0)\, t) \end{pmatrix} \vec{M}(0) = \mathbf{C}_X(\alpha_1 M_1(0)t)\vec{M}(0). \tag{2.72}$$

We obtain a similar equation for $\vec{R}$:

$$\frac{d}{dt}\vec{R} = \vec{R} \times \begin{pmatrix} \alpha_1 M_1 \\ 0 \\ 0 \end{pmatrix}, \tag{2.73}$$

and,

$$\vec{R}(t) = \mathbf{C}_X(\alpha_1 M_1(0)t)\vec{R}(0). \tag{2.74}$$

The configuration matrix evolves according to:

$$\mathbf{C}(t) = \mathbf{C}(0)\mathbf{C}_X^{-1}(\alpha_1 M_1(0)t). \tag{2.75}$$

Similarly, the Hamiltonians H_{M_2} and H_{M_3} lead to rotations about axis Y and Z:

1. $H_{M_2} \rightarrow \vec{M}(t) = \mathbf{C}_Y(\alpha_2 M_2(0)t)\, \vec{M}(0);\ \mathbf{C}(t) = \mathbf{C}(0)\mathbf{C}_Y^{-1}(\alpha_2 M_2(0)\, t);$

2. $H_{M_3} \rightarrow \vec{M}(t) = \mathbf{C}_Z(\alpha_3 M_3(0)t)\, \vec{M}(0);\ \mathbf{C}(t) = \mathbf{C}(0)\mathbf{C}_Z^{-1}(\alpha_3 M_3(0)\, t),$

where $\mathbf{C}_Y$ and $\mathbf{C}_Z$ refer to rotations about axis Y and Z respectively.

2.6.3 The Free Rigid Body as We See it

The function $H_{Axisymmetric}$ is the Hamiltonian of a body that is symmetric about Z; it was integrated in section 2.6.1. The function $H_{Triaxial}$ is a quadratic monomial of the form $H_{Triaxial} = \alpha_1 \frac{M_1^2}{2}$, where $\alpha_1 = (\frac{1}{I_1} - \frac{1}{I_2})$; it was integrated in section 2.6.2. Using

the method of WH91, we construct algorithms for the integration of the motion of a free rigid body, by stringing together the parts we have just integrated. The order of the algorithms is limited only by the computational effort that one is willing to spend.

The scheme conserves the magnitude of $\vec{M}$: the motion is a composition of orthogonal transformations. Also, the scheme preserves the spatial angular momentum vector $\vec{m}$: in every step $\mathcal{B}$ and $\vec{M}$ rotate by equal and opposite amounts. It is also true that the mapping is symplectic and area preserving on the angular momentum sphere, since it was derived from the Lie-Poisson structure, which was derived by reducing the canonical Poisson bracket from the six dimensional phase space to the sphere. The use of Cartesian coordinates avoids the singularities of Euler type angles. Finally, the configuration of the rigid body is recovered naturally as part of the integration.

2.6.4 Stability Analysis of the Free Rigid Body Algorithm

We are interested in the stability of the rigid body algorithm. By that we mean the conditions under which the algorithm faithfully renders the actual motion. Since the algorithm is symplectic, and the angular momentum vector is restricted to a sphere, we know that, for small enough step size, the angular momentum vector will not drift on the sphere. It will either follow a closed curve, or be confined by such curves. However, the motion could still suffer from resonant interactions between the frequencies of the system and the step size of the mapping. Such resonances are best understood via the time dependent Hamiltonian which our scheme integrates. In this section, we follow the work of Wisdom and Holman [52] on the stability of symplectic mappings for the gravitational n-body problem. We study the Hamiltonian that generates the first order mapping. We concentrate here on the primary resonances. The mapping Hamiltonian is

$$H_{map} = \frac{1}{2I_2}G^2 + \frac{1}{2}(\frac{1}{I_3} - \frac{1}{I_2})L^2 - 2\pi\delta_{2\pi}(\Omega t)\,\frac{1}{2}(\frac{1}{I_2} - \frac{1}{I_1})(G^2 - L^2)\sin^2(l). \qquad (2.76)$$

As in previous sections, $\delta_{2\pi}(t)$ is a periodic sequence of Dirac delta functions, with period 2π and Ω is the mapping frequency. The step size of the integrator is given by $h = 2\pi/\Omega$. The periodic delta functions admit a Fourier representation:

$$\delta_{2\pi}(t) = \frac{1}{2\pi} \sum_{n=-\infty}^{\infty} \cos(nt), \tag{2.77}$$

which we incorporate into H_{map}:

$$\begin{aligned} H_{map} &= \frac{1}{2I_2}G^2 + \frac{1}{2}(\frac{1}{I_3} - \frac{1}{I_2})L^2 \\ &- \frac{1}{4}(\frac{1}{I_2} - \frac{1}{I_1})(G^2 - L^2) \sum_{n=-\infty}^{\infty} \cos(n\Omega t) \\ &+ \frac{1}{4}(\frac{1}{I_2} - \frac{1}{I_1})(G^2 - L^2) \sum_{n=-\infty}^{\infty} \cos(2l - n\Omega t). \end{aligned} \tag{2.78}$$

Because the total angular momentum G is conserved we can restrict our attention to the dynamics of the canonical pair (l, L), and ignore constant terms in the Hamiltonian. We can further simplify the Hamiltonian by factoring $\frac{1}{I_3} - \frac{1}{I_2}$ out, and rescaling time to get:

$$H_{map} = \frac{L^2}{2} - 2\pi\delta_{2\pi}(\frac{\Omega}{\alpha}t)\frac{\gamma(G^2 - L^2)}{4} + \frac{\gamma(G^2 - L^2)}{4} \sum_{n=-\infty}^{n=\infty} \cos(2l - n\frac{\Omega}{\alpha}t) \tag{2.79}$$

where $\alpha = \frac{1}{I_3} - \frac{1}{I_2}$, and $\gamma = (\frac{1}{I_2} - \frac{1}{I_1})/\alpha$. We will concentrate on the case where $\gamma \ll 1$, i.e. when the problem differs from an integrable one by a small time dependent perturbation.

A primary resonance occurs whenever the argument of one of the cosines, in the Fourier expansion of H_{map}, is stationary: $2\frac{d}{dt}l - n\frac{\Omega}{\alpha} = 0$, for some $n \in \mathbf{Z}$. In order to study the motion near the n-th primary resonance, we extract the resonance Hamiltonian:

$$H_{res} = \frac{2 + \gamma}{4}L^2 + \frac{\gamma(G^2 - L^2)}{4}\cos(2l - n\frac{\Omega}{\alpha}t), \tag{2.80}$$

and ignore the other terms. The resonance Hamiltonian contains one linear combination of angles. We can eliminate the time dependence with a canonical transformation, whose generating function is:

$$F(L, \phi, t) = -\frac{1}{2}(L - L_r)(\phi + n\frac{\Omega}{\alpha}t), \tag{2.81}$$

where (p, ϕ) is the new canonical pair, and L_r is a constant to be determined. Explicitly, the transformation is given by:

$$\begin{aligned} p &= \frac{L - L_r}{2} \\ l &= \frac{1}{2}\left(\phi + n\frac{\Omega}{\alpha}t\right) \end{aligned} \tag{2.82}$$

Replacing in H_{res}, we get a time independent Hamiltonian:

$$\hat{H}_{res} = H_{res} + \frac{\partial F}{\partial t} = \frac{2+\gamma}{4}(2p + L_r)^2 + \frac{\gamma\left[G^2 - (2p + L_r)^2\right]}{4}\cos(\phi) - n\frac{\Omega}{\alpha}p. \tag{2.83}$$

Expecting small excursions away from the center of the resonance, we ignore terms of order γp and γp^2. We choose L_r to eliminate linear terms in p:

$$L_r = \frac{n\Omega}{2\alpha}. \tag{2.84}$$

The momentum L_r gives the angular momentum at the resonance. Since $|L| \leq G$, we must have $\frac{2|\alpha|G}{\Omega} \geq 1$ for primary resonances to exist, or $h \geq h_0 = \frac{\pi}{|\alpha|G}$. Ignoring the constant terms in $\hat{H}_{res}$, we get:

$$\hat{H}_{res} = 2p^2 + \frac{\gamma(G^2 - L_r^2)}{4}\cos(\phi) \tag{2.85}$$

The half-width of the libration region of this pendulum-like Hamiltonian is

$$p_{max} = \frac{\sqrt{\gamma(G^2 - L_r^2)}}{2}, \tag{2.86}$$

which we express in terms of the original variables:

$$L_{max} = 2p_{max} + L_r. \tag{2.87}$$

Notice that the maximum width is of the order of $\sqrt{\gamma}$.

Next, we look for the condition on Ω under which the separation between the resonance centers is equal to the sum of the half-width of their respective separatrices. This condition, known as the resonance overlap criterion, was used by Chirikov [10] as a heuristic criterion for the development of chaos in nonintegrable problems. Since we are concerned with the numerical reliability of the method, we will worry about the

overlap between the $n = 0$ resonance, which enters the actual motion, and the $n = 1$ resonance, which was introduced by the discretization. The condition for resonance overlap reads:

$$2p_{max}^{(0)} + 2p_{max}^{(1)} \geq |L_r^{(1)}|, \tag{2.88}$$

or,

$$\sqrt{\gamma}\left[G + \sqrt{G^2 - (\frac{\Omega}{2\alpha})^2}\right] \geq -\frac{\Omega}{2\alpha}. \tag{2.89}$$

In terms of the stepsize, the resonances will overlap when:

$$h \geq h_{RO} = -\frac{\pi(1+\gamma)}{2\sqrt{\gamma}\alpha G}. \tag{2.90}$$

The evolution can be affected by stepsize resonances even if there is no serious resonance overlap. Thus, a more conservative limit on the stepsize of the map is to require that there are no primary stepsize resonances in the phase space: $h \leq h_0$.

2.6.5 Numerical Tests of the Free Rigid Body Algorithm

The numerical experiments discussed in this section are intended to illustrate the conservation properties of the rigid body algorithm, and the spurious resonances introduced by the discretization.

The continuous free rigid body motion conserves the kinetic energy. For an axisymmetric body, the mapping is exact and consequently conserves the energy explicitly. However, for a triaxial body our free rigid body algorithm was not designed to explicitly conserve the energy. We expect that in this case the energy will oscillate with an amplitude that changes algebraically with the stepsize, for small enough stepsize. To illustrate this, we explored the dependence of the energy error on step size, with a first order implementation of the algorithm. The behavior of the energy error as a function of time is shown in Fig.2-1 for a rigid body which is close to axisymmetric: $I_1 = 0.5$, $I_2 = 0.51$, $I_3 = 1.0$. The initial conditions for this trajectory are: $M_2 = 0.0$, and $M_3 = 0.999$, with $M = 1.0$. The step size is $h = 0.01T_{prec}$, where $T_{prec} = 2\pi/(\alpha M_3(0))$, and $\alpha = 1/I_2 - 1/I_3$. As expected, the error oscillates and over the displayed time interval does not appear to grow secularly. As can be seen in the

mapping Hamiltonian of the previous section, the smaller the triaxiality of the rigid body, the smaller the energy error at a given stepsize.

Of course, the amplitude of the energy error varies with the stepsize. For this first order version of the algorithm, the energy error is linear with stepsize for small stepsize. At large stepsizes, stepsize resonances are encountered which give large energy errors. This behavior is illustrated in Fig. 2-2 for the same physical parameters and initial conditions as in the previous example. The maximum energy error over 5×10^3 iterations is plotted versus stepsize. The peaks in the energy error occur at stepsize resonances. Our stability analysis predicts primary resonances at stepsizes $h/T_{prec} = nM_3(0)/2$. Fig. 2-2 confirms the prediction.

Next we look at the conservation of the spatial angular momentum vector. Using the same rigid body but a second order version of the algorithm, we consider a trajectory with $M_1(0) = 0$, $M_2(0) = 0.6$, $M_3(0) = 0.8$, and an initial configuration which coincides with the inertial frame. The free body algorithm is designed to conserve the spatial angular momentum vector, $\vec{m}$, and a fortiori, the magnitude of that vector. However, in practice, roundoff errors creep up on the integrals. As shown in Fig. 2-3, the magnitude of $\vec{m}$ differed from unity by $O(10^{-11})$ after a period of 10^7 T_{prec}. As far as the spatial components of $\vec{m}$ are concerned, they are affected both by roundoff errors in $\vec{M}$ and in the configuration. The configuration could be followed either in terms of the standard rotation matrices or in terms of the quaternions equivalent to them (see, for example, [19]). It is questionable whether quaternions alone can help cut down on the round-off errors, since one pays the price for carrying four scalars (instead of the nine required for matrices) in terms of more involved algebraic operations. However, since our quaternions are of unit magnitude, we can enforce the special orthogonality of our transformations by normalizing at regular intervals. Typically, we find that by normalizing the quaternions, Fig. 2-4, we can cut round-off errors by one order of magnitude below the maximum errors accrued when we used standard rotation matrices, Fig. 2-5. Thus, using normalized quaternions does cut down on roundoff error, but we suspect more improvement can still be made.

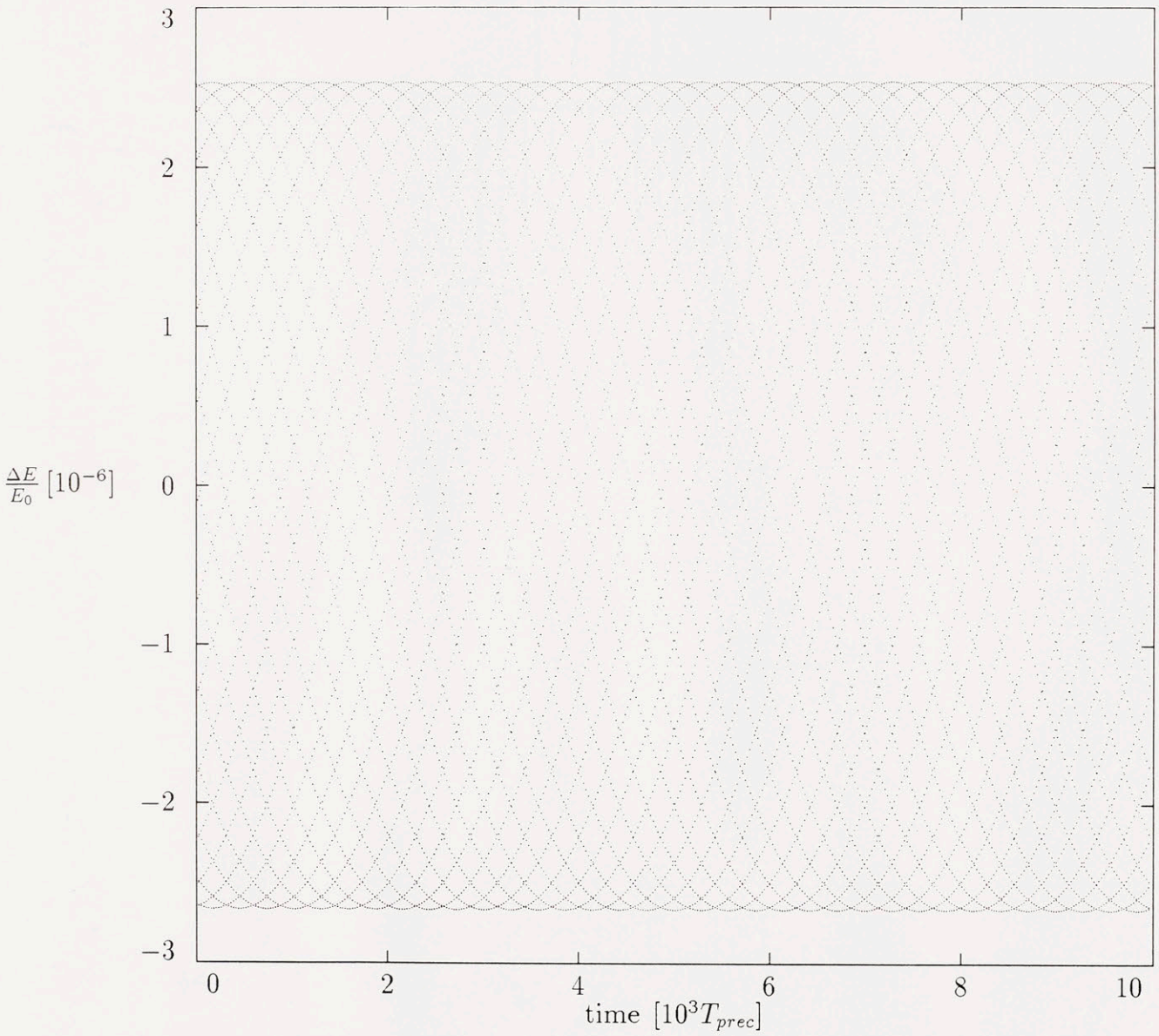

Figure 2-1: The energy error in the free rigid body algorithm is plotted against time. The stepsize was set at 1/100 of the axisymmetric precession frequency, T_{prec}.

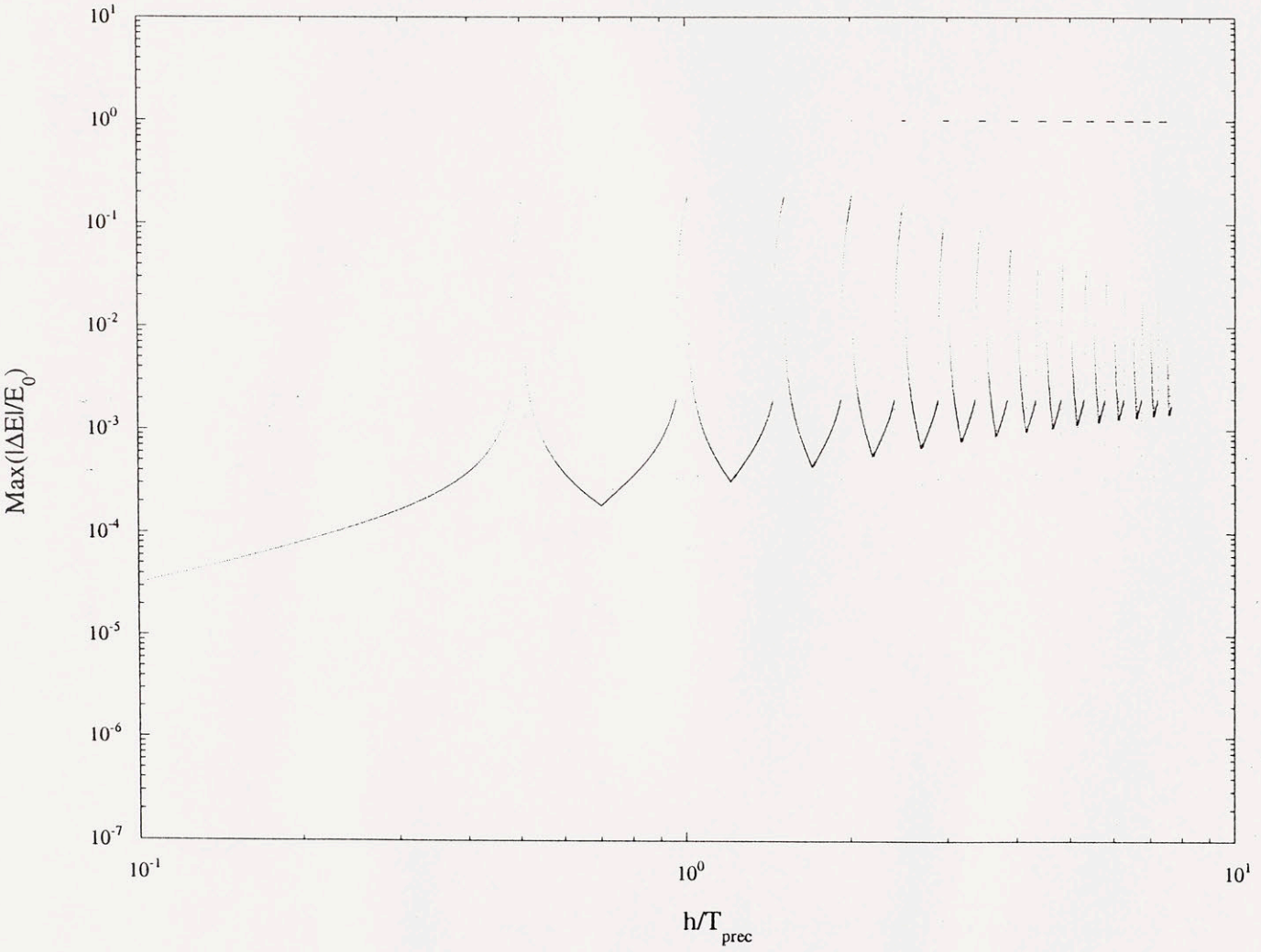

Figure 2-2: The maximum energy error realized in 5×10^3 iterations, in a first order algorithm, is plotted against the step size. Energy jumps occur at stepsizes close to $nT_{prec}/2$, where n is the order of the primary resonance

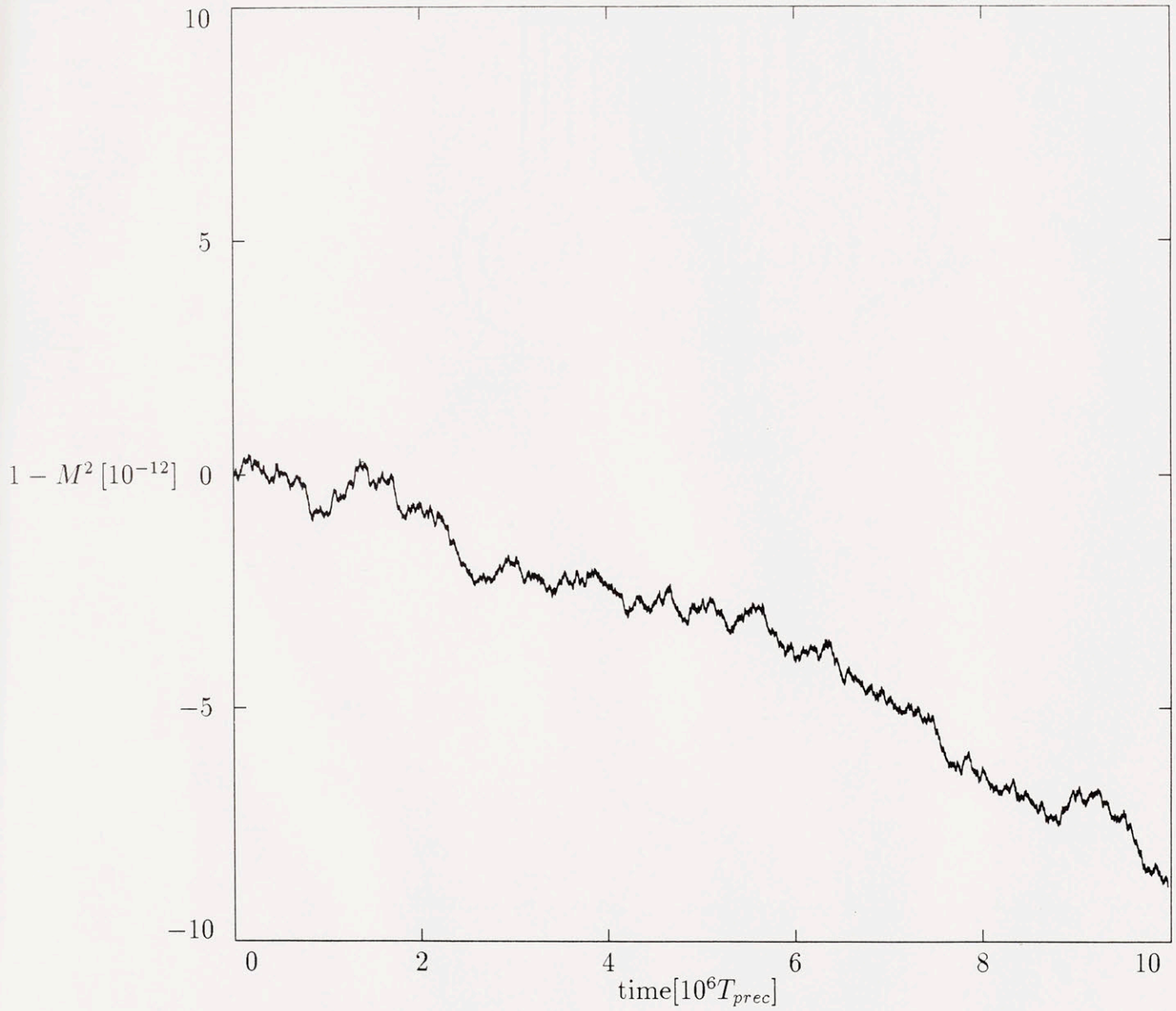

Figure 2-3: A free rigid body was followed with a second order algorithm. The error in the magnitude of the angular momentum vector is plotted against time.

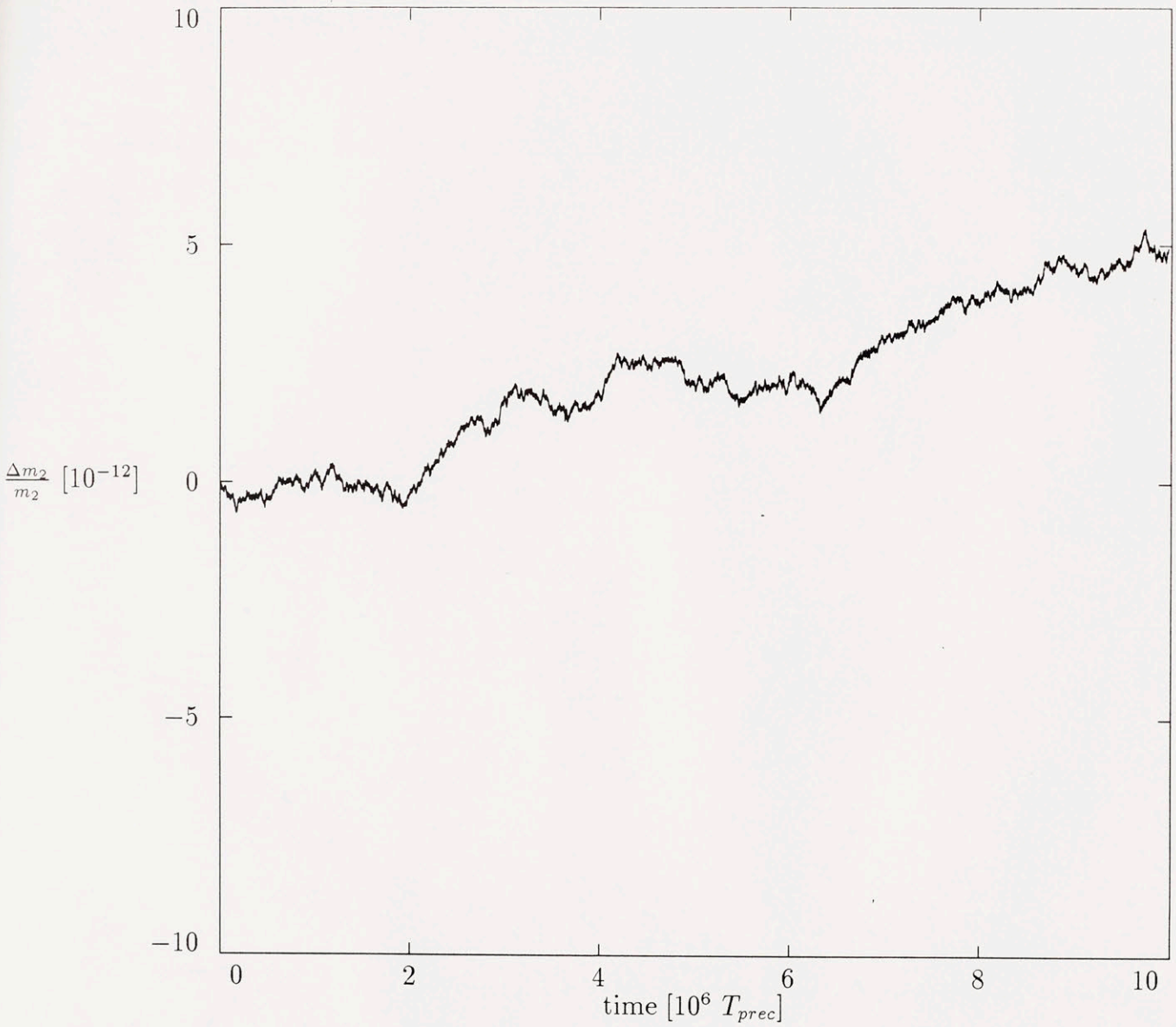

Figure 2-4: The angular momentum of a free rigid body is fixed in space. Here, we plot the error in m_2, the y spatial component of the angular momentum vector, against time. In this experiment, the configuration is represented in terms of quaternions which are normalized every 100 steps

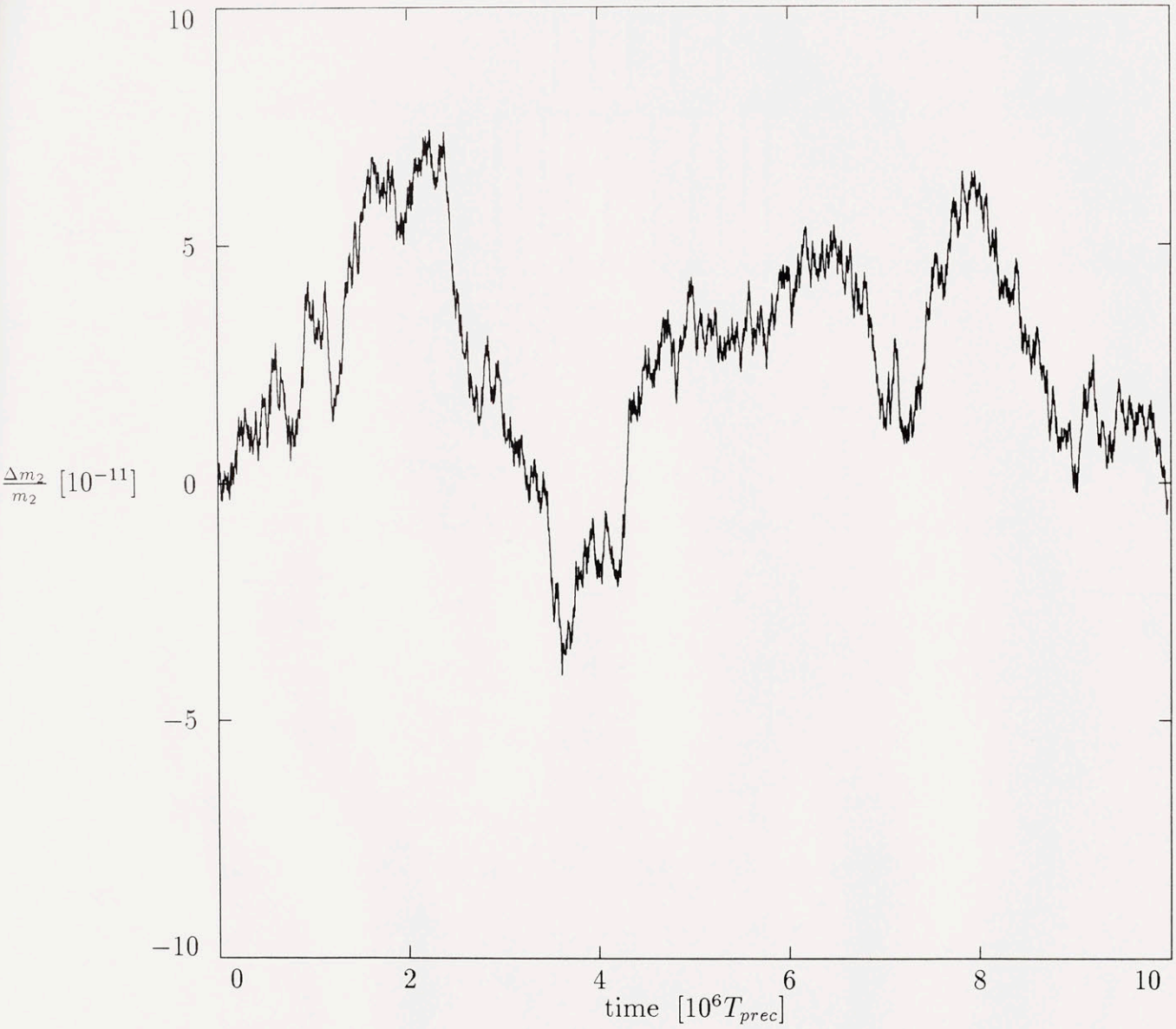

Figure 2-5: The same experiment as in Fig.4 was carried out except that in this case the configuration is represented in terms of standard rotations.

In summary, the energy integral is conserved to the order of the algorithm, as long as the chosen step size, for a given trajectory, avoids the artificial resonances. The angular momentum integrals suffer only from roundoff errors, and care must be taken to reduce them. Writing the evolution of the configuration in terms of quaternions is useful in the struggle against roundoff errors.

2.7 Lie-Poisson Integrator for a Rigid Body in the Field of a Mass Point

Having developed algorithms for the free rigid body, we now turn to the solution of the interaction Hamiltonian $\hat{H}_{Interaction}$

$$\hat{H}_{Interaction} = -\frac{Gm_1}{2R^3} tr(\mathbf{I}) + \frac{3}{2}\frac{Gm_1}{R^5}\vec{R}\cdot\mathbf{I}\vec{R} \tag{2.91}$$

to complete the full spin-orbit map.

Using the spin-orbit Lie-Poisson bracket, the equations of motion are:

$$\begin{aligned}
\frac{d}{dt}\vec{R} &= 0, \\
\frac{d}{dt}\vec{P} &= -\frac{3Gm_1}{2R^5} tr(\mathbf{I})\vec{R} - \frac{3Gm_1}{R^5}\mathbf{I}\vec{R} + \frac{15Gm_1}{2R^7}\left(\vec{R}\cdot\mathbf{I}\vec{R}\right)\vec{R}, \\
\frac{d}{dt}\vec{M} &= \frac{3Gm_1}{R^5}\vec{R}\times\mathbf{I}\vec{R},
\end{aligned} \tag{2.92}$$

where $tr(\mathbf{I})$ stands for the trace of the inertia tensor.

Since, $\frac{d}{dt}\vec{R} = 0$, we trivially integrate the differential equations:

$$\begin{aligned}
\vec{R}(t) &= \vec{R}(0), \\
\vec{P}(t) &= \vec{P}(0) + [\vec{\nabla}_{\vec{R}}\hat{H}_{Interaction}]\, t \\
\vec{M}(t) &= \vec{M}(0) + [\vec{R}(0)\times\vec{\nabla}_{\vec{R}}\hat{H}_{interaction}]\, t,
\end{aligned} \tag{2.93}$$

The forces and the torques are evaluated at $\vec{R}(0)$, the relative position vector in the body frame $\mathcal{B}$. Since the configuration is not affected by the evolution generated by $H_{Interaction}$, we can assume that the configuration matrix at time t is given, and invert to get $\vec{R}(t) = \mathbf{C}^T(t)\vec{r}(t)$. It is natural to compute the Keplerian evolution in

an inertial frame, so the change in the linear momentum in the inertial frame must be monitored:

$$\vec{p}(t) = \vec{p}(0) + \mathbf{C}(t)(P(t) - P(0)). \tag{2.94}$$

Having integrated all the components of the spin-orbit Hamiltonian, we are in a position to construct algorithms for the motion of a rigid body gravitationally interacting with a mass point. The simplest algorithm is first order in time and consists of a step of Kepler and Euler and a step of potential interactions. One can construct an algorithm which is second order in time by taking a half step of Eulerian and Keplerian motion, followed by a full step of potential interactions, and ending with a half step of Eulerian and Keplerian motion. An Euler step updates the configuration of the rigid body which can then be used to compute the interactions in the rigid body frame.

If one is interested in a situation where the effect of the rigid body on the orbit of the mass point is negligible, then all that one has to do is to neglect the part of the interaction that affects the linear momenta. Of course, in that case, the total angular momentum is no longer conserved, but the orbital angular momentum is. Such a situation arises in the study of spin orbit coupling in the solar system. It has been investigated in detail in [48, 50]. Our algorithm presents an efficient tool for dealing with this problem.

As an algorithm for Lie-Poisson dynamics, ours echoes the generalizations of the ideas of Forest and Ruth [17] given in Channell and Scovel ([9], hereafter CS91). These ideas are equivalent to the operator splitting approach given in WH91 with a different motivation. However, CS91 limit themselves, with Forest and Ruth [17], to Hamiltonians which can be written as the sum of a kinetic and a potential energy. The approach of WH91 and our generalization to Lie-Poisson dynamics are not limited to such Hamiltonians. Also, CS91 do not consider the splitting of integrable problems into efficiently integrable subproblems, a step we exploit in our derivation. Furthermore, the approach of WH91 has the added advantage of giving us a handle on the time dependent Hamiltonian that is exactly integrated by the algorithm. This Hamiltonian can in turn be used to analyze the structure of the spurious resonances

introduced by the algorithm as was done in Wisdom and Holman [52] and carried out for the rigid body map in section 2.6.4. Finally, CS91 presented efficient implementations of the approach of Ge and Marsden [18] which involves an approximation of the dynamics via generating functions. However, as pointed out by CS91 the explicit algorithms which use the operator splitting route are, in general, faster than algorithms that use the generating functions approach.

As an algorithm for rigid body dynamics, ours differs from the one presented in Austin, Krishnaprasad, and Wang [5] on the ground that our algorithm is Lie-Poisson while theirs, which is based on the mid-point rule, only preserves the Lie-Poisson structure to second order in the step size. The mid-point rule provides second order algorithms which conserve integrals of motion which are linear or quadratic in the coordinates. In that sense, the algorithm of Austin et.al [5] preserves both the energy and the angular momentum of the free rigid body. However, while it traces the trajectories on the sphere, it suffers from a systematic lag in the configuration space. Since our applications have an energy which is not quadratic in the coordinates, the mid-point rule will not preserve the energy anyway, and then it becomes advantageous to have the Lie-Poisson structure preserved. Furthermore, Austin et.al [5] do not provide higher order generalizations of their algorithms. To our knowledge none of these rigid body algorithms have been generalized to spin-orbit problems as considered in this paper.

2.7.1 Energy Conservation in the Spin-Orbit Integrator

We explore the energy conservation properties of the spin-orbit coupling algorithm. In most solar system applications, the rotational energy is negligible when compared to the orbital energy. To get a handle on the rigid body contribution to the energy, we look at a rigid body moving on a fixed Keplerian orbit. Of course, in this case, neither the total energy nor the total angular momentum vector are conserved. However, by choosing the orbit to be circular, and moving to a frame that is rotating at the orbital rate, we get rid of the periodic time dependence, and obtain a "Jacobi"-like integral which captures the contribution of rigid body interactions to the energy (see [50]). As

an example we considered a body with the Moon's moments of inertia which is moving on a fixed circular orbit and use a second order version of the algorithm. We started the body spinning at the orbital frequency about the axis with largest principal moment, and tipped that axis 0.1 radians with respect to the orbit normal. We monitored the variation in the integral of the motion over a time span of 5000 orbits, with a step size of 1/100 of the orbital period. The result is shown in Fig. 2-6. The error in energy oscillates and shows no signs of growth, a commonly observed feature of symplectic integrators. We carried out a similar experiment with an axisymmetric Mars-like body spinning about the axis with largest principal moment at Mars' current rotational period and attitude. With a stepsize of 1/100 of the orbital period, the energy oscillated with an amplitude of order 10^{-11} as can be seen in Fig. 2-7.

2.8 The Dynamics of Rigid Bodies in the Solar System

Now that we have derived a mapping for following the motion of a rigid body gravitationally interacting with a mass point, it is a simple matter to generalize to more complicated situations.

2.8.1 One Rigid Body in the Gravitational n-Body Problem

The step from one mass point and a rigid body to n mass points and a rigid body increases the computational effort, but leaves the conceptual framework practically unchanged. The Hamiltonian of this problem is given by:

$$H = \frac{1}{2}\vec{M}\cdot\mathbf{I}^{-1}\vec{M} + \sum_{i=0}^{n}\frac{p_i^2}{2m_i} - \sum_{0\le i<j}^{n}\frac{Gm_im_j}{r_{ij}} - \sum_{\substack{i=0\\ i\neq 1}}^{n}\int_B \frac{Gm_i}{|r_{i1}+\mathbf{C}\vec{Q}|}dm(\vec{Q}), \qquad (2.95)$$

where, in this case, the massive central body has index 0 and the rigid body has the index 1. We carry out the following operations on the Hamiltonian:

- Transform the Hamiltonian to heliocentric (or Jacobi) coordinates to eliminate the center of mass motion;

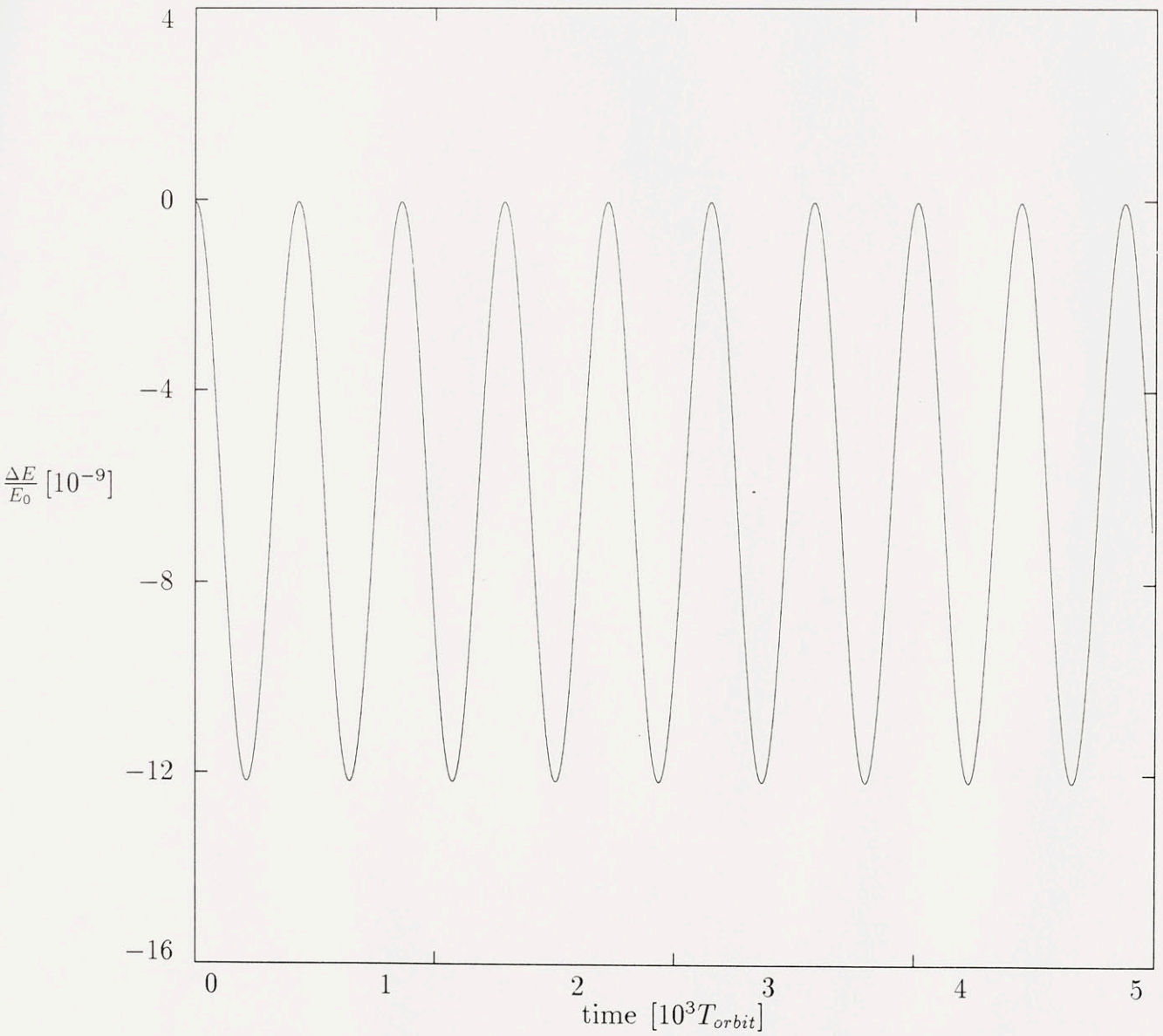

Figure 2-6: The error in the "Jacobi" integral of a Moon-like body moving on a fixed circular orbit is plotted against time.

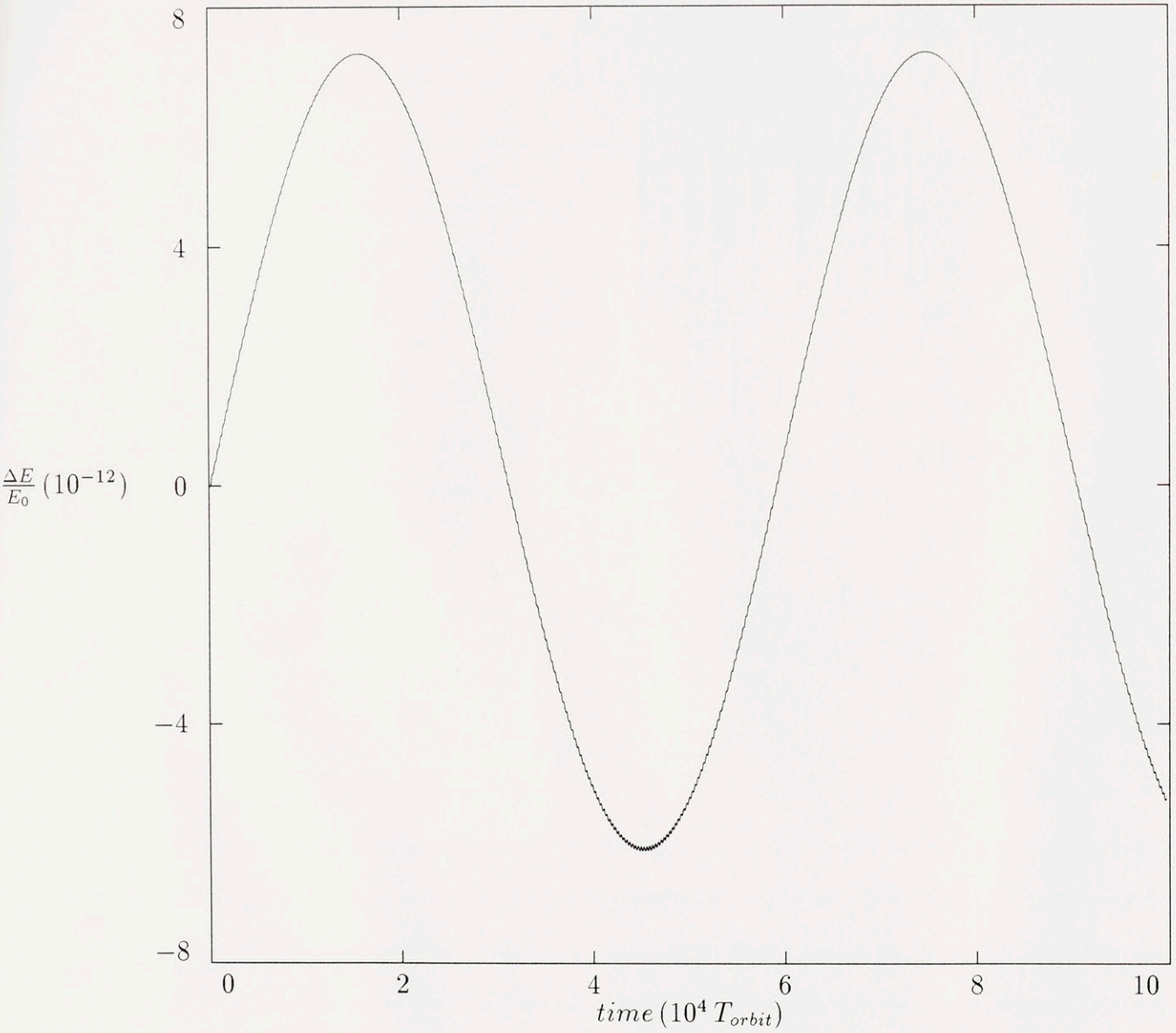

Figure 2-7: The error in the "Jacobi" integral of a Mars-like body moving on a fixed circular orbit is plotted against time.

- Further transform the Hamiltonian by moving to a frame rotating with the rigid body;
- Expand the potential interaction between the rigid body and the mass points in terms of Legendre polynomials and keep, as before, three terms of the expansion;
- Group into two separate Hamiltonians the terms governing the free motion (Keplerian and Eulerian), and the interactions (translational and rotational).

We work in a heliocentric framework since it is natural for computing the rigid body interactions. We carry out the steps outlined above and end up with the following Hamiltonian:

$$\hat{H} = \hat{H}_{Kepler} + \hat{H}_{Euler} + \hat{H}_{Interactions} + \hat{H}_{Indirect}, \tag{2.96}$$

where,

$$\begin{aligned}
\hat{H}_{Kepler} &= \sum_{i=1}^{n} \left[\frac{\vec{P}_i^2}{2\mu_i} - \frac{Gm_0 m_i}{R_{0i}} \right] \\
\hat{H}_{Euler} &= \frac{M_1^2}{2I_1} + \frac{M_2^2}{2I_2} + \frac{M_3^2}{2I_3} \\
\hat{H}_{Interactions} &= -\sum_{0<i<j}^{n} \frac{Gm_i m_j}{R_{ij}} - \sum_{\substack{i=0 \\ i\neq 1}}^{n} \left[\frac{Gm_i}{2R_{i1}^3} tr(\mathbf{I}) - \frac{3}{2} \frac{Gm_i}{R_{i1}^5} \vec{R}_{i1} \cdot \mathbf{I} \vec{R}_{i1} \right] \\
\hat{H}_{Indirect} &= \frac{1}{2m_0} \sum_{\substack{i,j=1 \\ j\neq i}}^{n} \vec{P}_i \cdot \vec{P}_j,
\end{aligned} \tag{2.97}$$

where $1/\mu_i = 1/m_i + 1/m_0$.

We note that the Lie-Poisson bracket that we derived for the case of a rigid body interacting with one mass point generalizes naturally to the case of n mass points. The reduction was made possible by moving to the rigid body frame, a step we can still take in this problem. All we have to do is to account for the additional torques on the body and the reaction forces on the mass points:

$$\begin{aligned}
\frac{d}{dt}\vec{R}_{0i} &= \left\{ \vec{R}, \hat{H} \right\} = \vec{R}_{0i} \times \vec{\nabla}_{\vec{M}} \hat{H} + \vec{\nabla}_{\vec{P}_i} \hat{H} \\
\frac{d}{dt}\vec{P}_i &= \left\{ \vec{P}, \hat{H} \right\} = \vec{P}_i \times \vec{\nabla}_{\vec{M}} \hat{H} - \vec{\nabla}_{\vec{R}_{0i}} \hat{H}, \; i = 1, \ldots, n \\
\frac{d}{dt}\vec{M} &= \left\{ \vec{M}, \hat{H} \right\} = \vec{M} \times \vec{\nabla}_{\vec{M}} \hat{H} + \sum_{j=1}^{n} \vec{R}_{0j} \times \vec{\nabla}_{\vec{R}_{0j}} \hat{H}.
\end{aligned} \tag{2.98}$$

The Keplerian motion is found by using a Kepler solver like the one discussed in WH91. The Eulerian free body motion is solved using the Lie-Poisson algorithm we presented above. The Hamiltonian $H_{Indirect}$ results from the transformation to the non-inertial heliocentric frame. Since it only depends on the linear momenta, it will only affect the position vectors:

$$\vec{R}_{0i}\ (t) = \vec{R}_{0i}\ (0) + \frac{t}{m_0} \sum_{\substack{j=1 \\ j \neq i}}^{n} \vec{P}_j\ ,\ \text{i =1,...,n} \tag{2.99}$$

The interaction Hamiltonian depends on the relative distances between the various objects. Thus, as before, this Hamiltonian affects the momenta only, leaving the position vectors and the configuration of the rigid body unchanged. We integrate it to get:

$$\begin{aligned} \vec{R}_{0i}(t) &= \vec{R}_{0i}(0) \\ \vec{P}_i(t) &= \vec{P}_i(0) - [\vec{\nabla}_{\vec{R}_{0i}} \hat{H}_{Interaction}]\, t,\ \ i = 1, \ldots, n, \\ \vec{M}(t) &= \vec{M}(0) + [\sum_{\substack{j=0 \\ j \neq 1}}^{n} \vec{R}_{j1}(0) \times \vec{\nabla}_{\vec{R}_{j1}} \hat{H}_{Interaction}]\, t, \end{aligned} \tag{2.100}$$

where the forces and torques are evaluated at $\vec{R}_{0i}(0)$, $i = 1, \ldots, n$.

This completes the integration of the parts. Finally, we construct a mapping that approximates solutions to the full Hamiltonian by following the method of WH91. A second order mapping will consist of: a half step along $H_{Interactions}$ which modifies the momenta; a half step along $H_{Indirect}$, which modifies the position vectors; a full step of Keplerian and Eulerian motion; a half step $H_{Indirect}$ with the current momenta and a final half step of $H_{Interactions}$.

2.8.2 Two or More Rigid Bodies in the Gravitational n-Body Problem

This case generalizes the previous one. We will be interested in cases where the first three Legendre polynomials in the potential expansion are sufficient. This allows us to ignore rigid-rigid interactions, or equivalently, to assume that each rigid body sees

all the other bodies in the system as mass points. Thus, the problem reduces to the previous one, except that we have to follow two or more angular momentum vectors and configurations instead of one.

2.9 Summary

We derived a symplectic integrator for a free rigid body, which conserves the magnitude of the angular momentum vector and its orientation in space. Two equivalent versions were discussed: one made use of a canonical Poisson structure, the other of the Lie-Poisson structure of a free rigid body. Numerical experiments explored the conservation properties of the algorithm. Round-off errors were reduced by using a quaternion formulation, with timely normalization. The energy error was bounded, and suffered from large increases at resonant stepsizes. The time dependent Hamiltonian, which generates the algorithm, was used to analyze the primary resonances introduced by the discretization. The free rigid body integrator was incorporated in the n body integrator of WH91, to provide a mapping for the dynamics of one or more rigid bodies interacting gravitationally with mass points. This mapping is Lie-Poisson in the sense that it preserves the Poisson structure and the symmetries generated by the Lie group of Euclidean transformations.

Chapter 3

The Obliquity of Mars: A Case of Adiabatic Chaos

It has been understood for some time, thanks to Ward's analysis of secular spin-orbit resonances, that the rotation of Mars is strongly affected by variations in its orbit.[41, 42, 44] The large variations in the obliquity of Mars predicted in some models would have important consequences for the modulation of Mars' climate and other atmospheric behavior such as dust storms. Variations of the obliquity have been suggested as a possible cause of the layered polar deposits on Mars.[39, 46] However, a number of obstacles have prevented a reliable determination of the history of the obliquity of Mars. One obstacle is fundamental and unavoidable. Ward, Burns, and Toon [45, 20] pointed out that a variety of physical mechanisms can change the moments of inertia of Mars, and that as the moments of inertia change secular spin-orbit resonances could be encountered which can drastically alter the obliquity of Mars. Secular spin-orbit resonances occur when the period of precession of the spin-axis of Mars is commensurate with one of the periods in the variation of the orbit of Mars. The timescale for significant internal geophysical changes in the physical rotational parameters of Mars is estimated to be greater than 100 million years, perhaps even billions of years. On shorter timescales, less than 100 million years, the most significant obstacle to a reliable determination of the history of the obliquity has been due to uncertainties in the orbital dynamics of Mars. The strongest secular spin-orbit res-

onance is due to the near equality of the frequency of the precession of the spin-axis with the frequency of the second inclination mode of the solar system, the mode that dominates the evolution of the orbit plane of Venus. As orbit theories have improved, the estimates of the difference between these frequencies have varied significantly.[23] Recently, Ward and Rudy [46] used an improved Fourier decomposition of the evolution of the orbit of Mars from the secular semi-numerical theory of Laskar [23] to update the history of the obliquity of Mars. They found that on a timescale of several million years the obliquity reaches values as large as 45°, compared to a maximum of 35° found using earlier orbit theories. Meanwhile, Laskar [24, 25] has found evidence that the evolution of the solar system is chaotic in a numerical integration of an averaged secular approximation of the equations of motion for the planets. Sussman and Wisdom [36] confirmed this result by direct numerical integration of the whole solar system. The timescale for exponential divergence is only about 4-5 million years. Thus the evolution of the planetary system is not quasiperiodic, and consequently not well described by Fourier series, an assumption made in all existing investigations of the obliquity of Mars. The discovery that the solar system is chaotic necessitates a new investigation of the evolution of the obliquity of Mars without Fourier approximations to the orbital variations. Here we present the results of a number of such direct numerical integrations of the rotation of Mars in the chaotically evolving planetary system.

3.0.1 Physical Model

Our physical model for the planetary evolution is the same as that used by Sussman and Wisdom [36], which is the same as Quinn, Tremaine, and Duncan [32] except for an unimportant difference in the treatment of the general relativistic corrections. In addition to the effects of general relativity, the model approximates the effect of the Earth-Moon quadrupole on the evolution of the planetary orbits. We take Mars to be an axisymmetric body. We consider both the case in which only the solar torques are included and the case where all gravitational torques are taken into account. We ignore the effect of Mars' extended shape on the evolution of the planetary orbits.

For the physical parameters of Mars we assume $J_2 = 0.00196$ [6, 21, 46], and $\lambda = C/MR^2 = 0.366$ [22, 21, 46]. We used two different sets of initial conditions. In set IC1 we took the initial conditions and masses from Quinn, Tremaine, and Duncan. In the other set IC2 we took initial conditions and masses from JPL ephemeris DE202 [35]. The rotational state of Mars was derived from M.E. Davies, et al. [13, 14]. We use the symplectic Lie-Poisson integration algorithm, which we discussed in the previous chapter to integrate the motion. The stepsize in our integrations is 7.2 days. Our integration extends backwards in time.

3.0.2 Numerical Integrations

Fig. 3-1 shows the obliquity of Mars, Θ, for 80 million years in the past as determined by our numerical integration with initial condition set IC1. The obliquity of Mars executes large irregular variations that range from about 11° to about 49°. We have computed the Lyapunov exponent for the spin dynamics and find that the evolution is chaotic with an exponential divergence timescale of about 3-4 million years.

The sudden change in mean obliquity that occurs about 4 million years ago (Fig. 3-2) is not a sensitive feature of the orbit model. The same transition occurs with initial condition set IC2. Indeed, the initial segment of both integrations is remarkably similar to that found by Ward and Rudy [46], including the transition in mean obliquity. Beyond about 7 million years in the past the obliquity in our calculation begins to diverge from that found by Ward and Rudy. In light of the chaotic evolution of the spin-axis such divergence is to be expected. Ward and Rudy use Laskar's Fourier representation of the orbit of Mars, which approximates the chaotic evolution of the orbit over about 10 million years [23, 46]. So if the chaotic orbit model of Laskar were used instead of the quasiperiodic representation of the orbit, we expect the obliquity of Mars would behave similarly. Thus the history of the obliquity of Mars over the last few million years is no longer sensitive to remaining differences in the models of the evolution of the orbit of Mars.

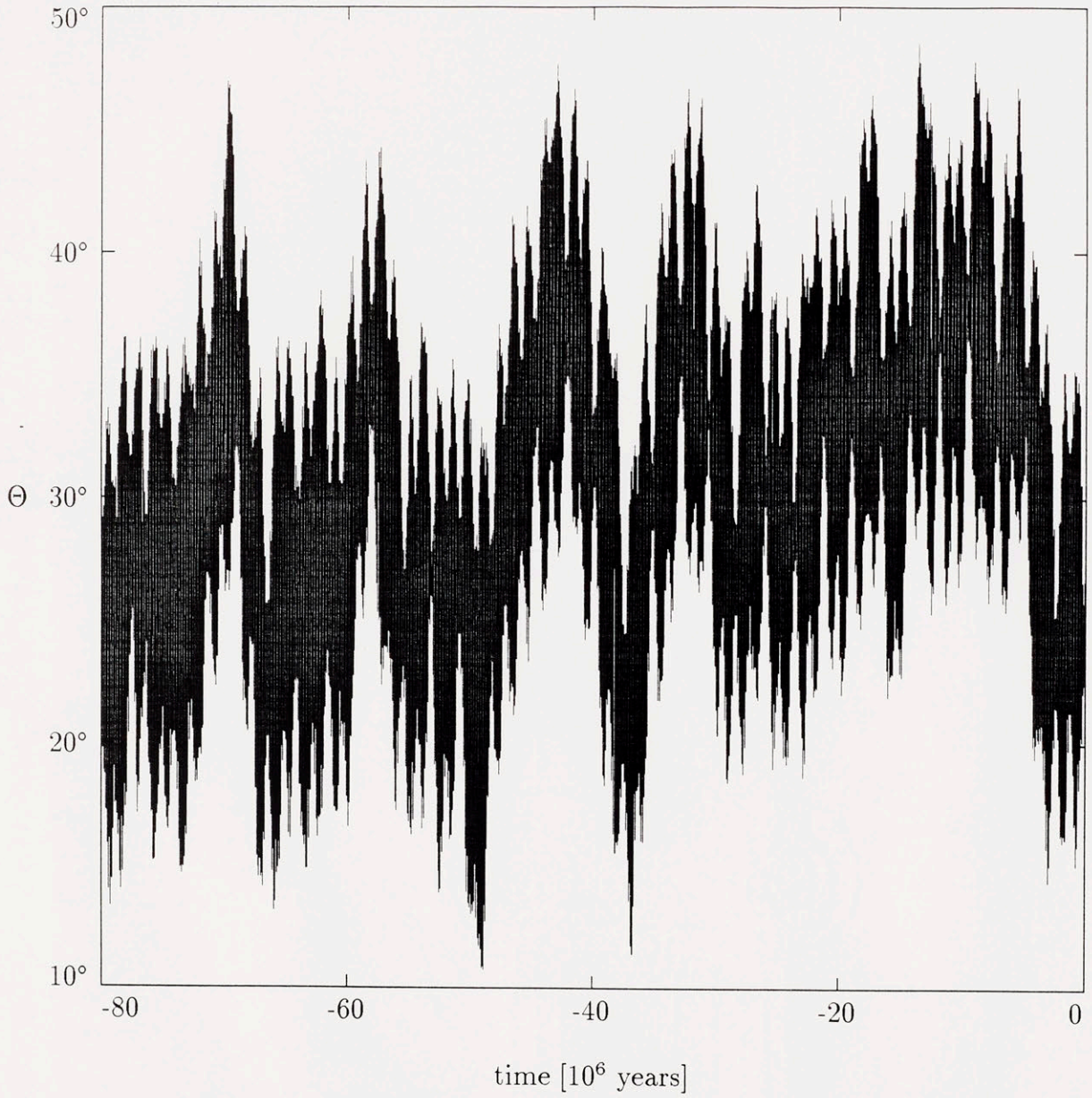

Figure 3-1: The obliquity of Mars for initial conditions IC1 over the last 80 million years has large chaotic variations.

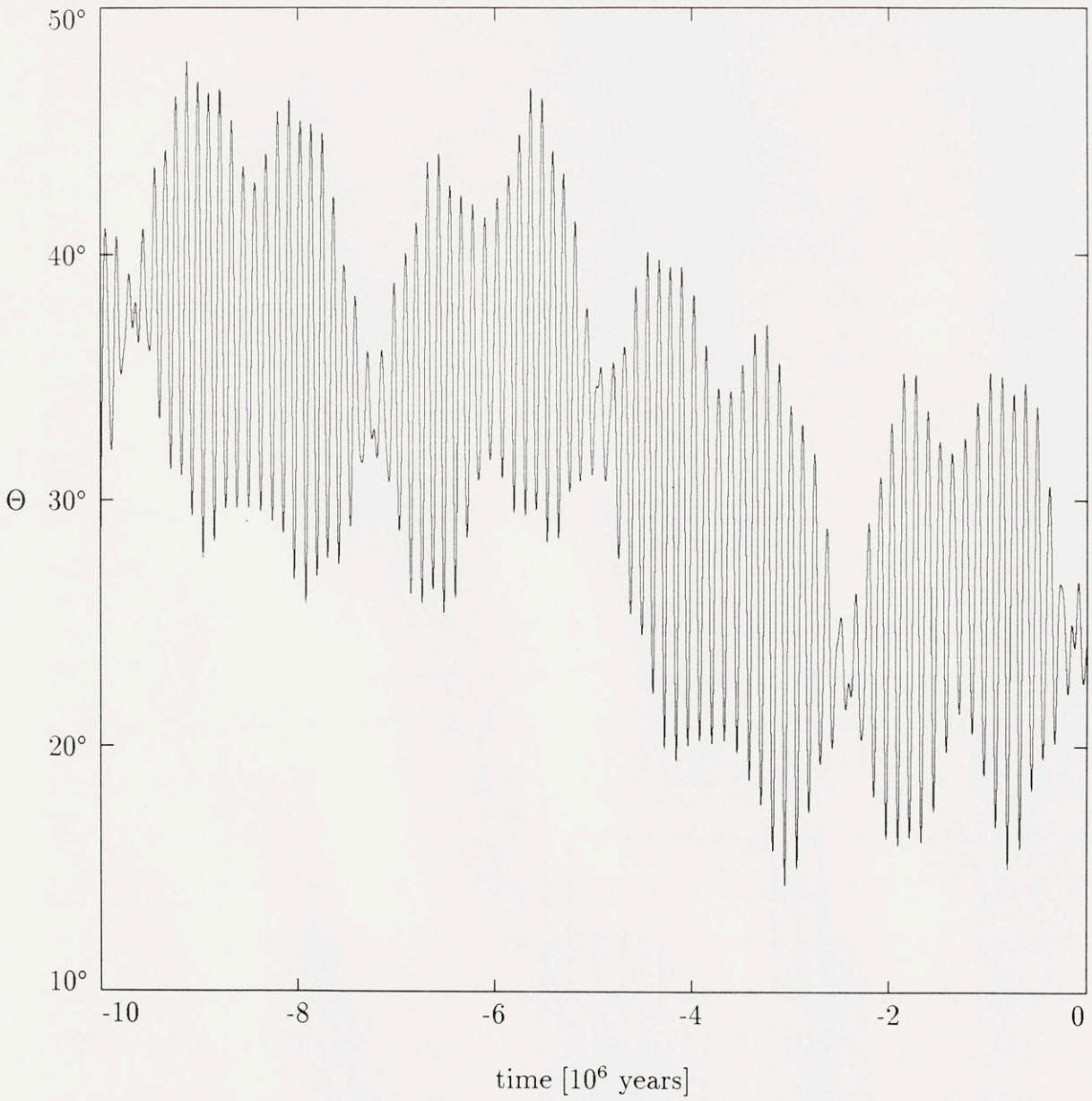

Figure 3-2: The obliquity of Mars over the last 10 million years shows a relatively abrupt transition about 4 million years ago.

3.0.3 Secular Spin-Orbit Resonance

Ward and Rudy [46] attributed the transition in mean obliquity to passage through a secular spin-orbit resonance. As mentioned above, the most important secular spin-orbit resonance for the evolution of the rotation of Mars is due to the near equality of the frequency of the precession of the spin-axis with s_2', the frequency of the second inclination mode of the solar system. In the Laskar Fourier decomposition of the evolution of the orbit of Mars, the component due to the second inclination mode is accompanied by a number of smaller components of similar frequency. A multiplet of components can be viewed as a single component with varying amplitude and frequency, the frequency of the variations being comparable to the frequency spread of the multiplet. Ward and Rudy pointed out that transitions across the resonance and capture into the resonance can be induced by this modulation. As the amplitude and frequency of the resonant perturbation vary, the amplitude of the resonance motion adjusts to approximately preserve the adiabatically invariant resonance action. If the modulation is great enough, transitions can be induced. A plot of the resonance angle $h_1 - \Omega_2^\circ$ versus time confirms the essential role this resonance plays in the dynamics (Fig. 3-3). Here, h_1 is the ascending node of the equator of Mars on the invariable plane, and Ω_2° is the phase of the second proper mode of the solar system computed from our data using the transformation of Laskar [25]. The transition in the mean obliquity that occurs about 4 million years ago coincides with a transition across the resonance associated with this combination of angles: the direction of rotation of the resonance angle changes as the mean obliquity changes. In Fig. 3-4 the mean obliquity, $\bar{\Theta}$, is plotted versus the resonance angle, $h_1 - \Omega_2^\circ$. The mean obliquity has been computed from the obliquity with a simple low-pass filter that removes frequencies above about 10 arcsec/year. As the resonance angle circulates the mean obliquity is relatively constant and stays on one side of the resonance; oscillation of the resonance variable is associated with an oscillation of the obliquity. This behavior is typical of non-linear resonance. Transition from circulation in one direction to circulation in the other direction is associated with a sudden change in the mean

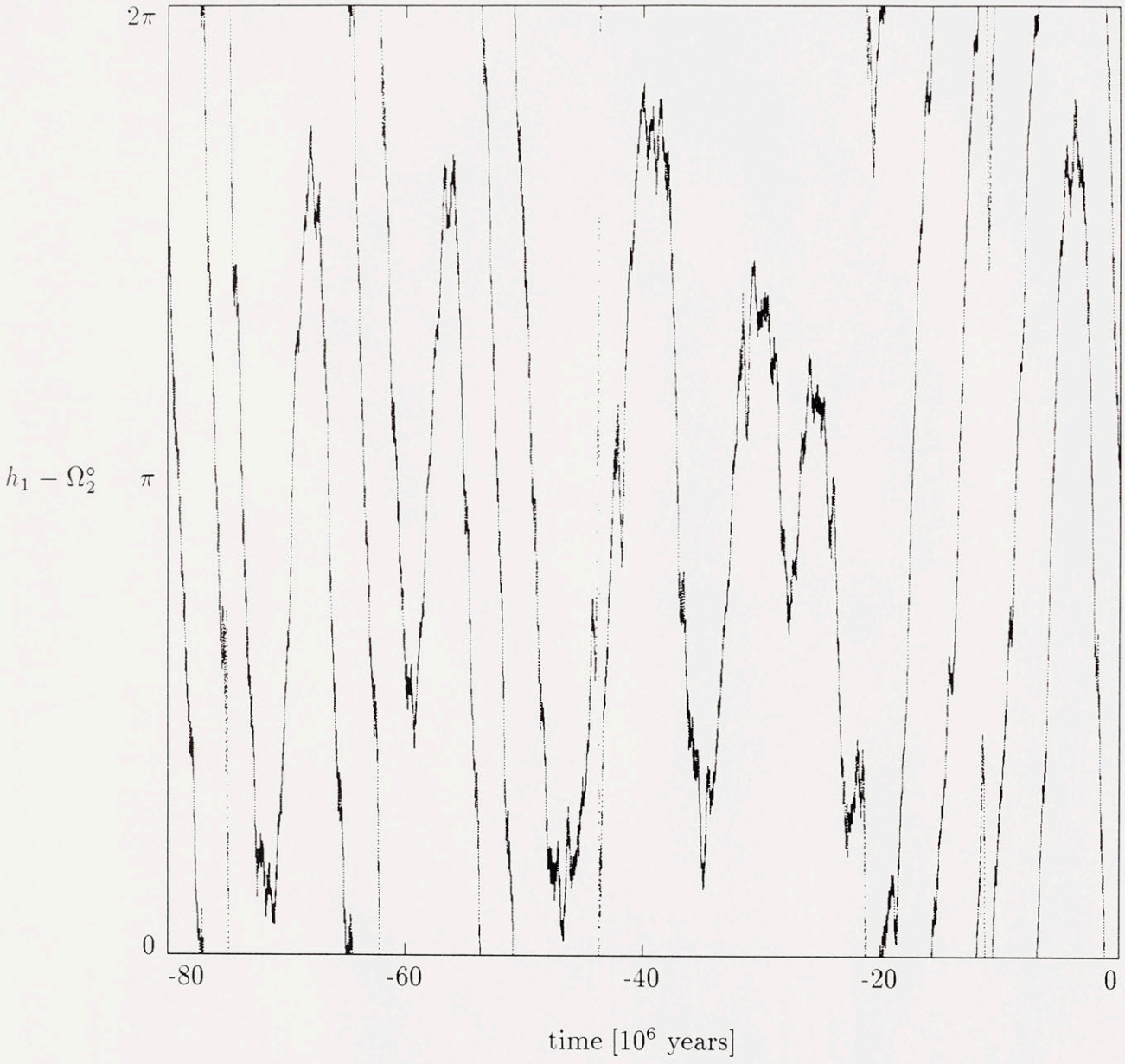

Figure 3-3: The longitude of the equator of Mars minus the phase of the second inclination proper solar system mode alternates between circulation and libration.

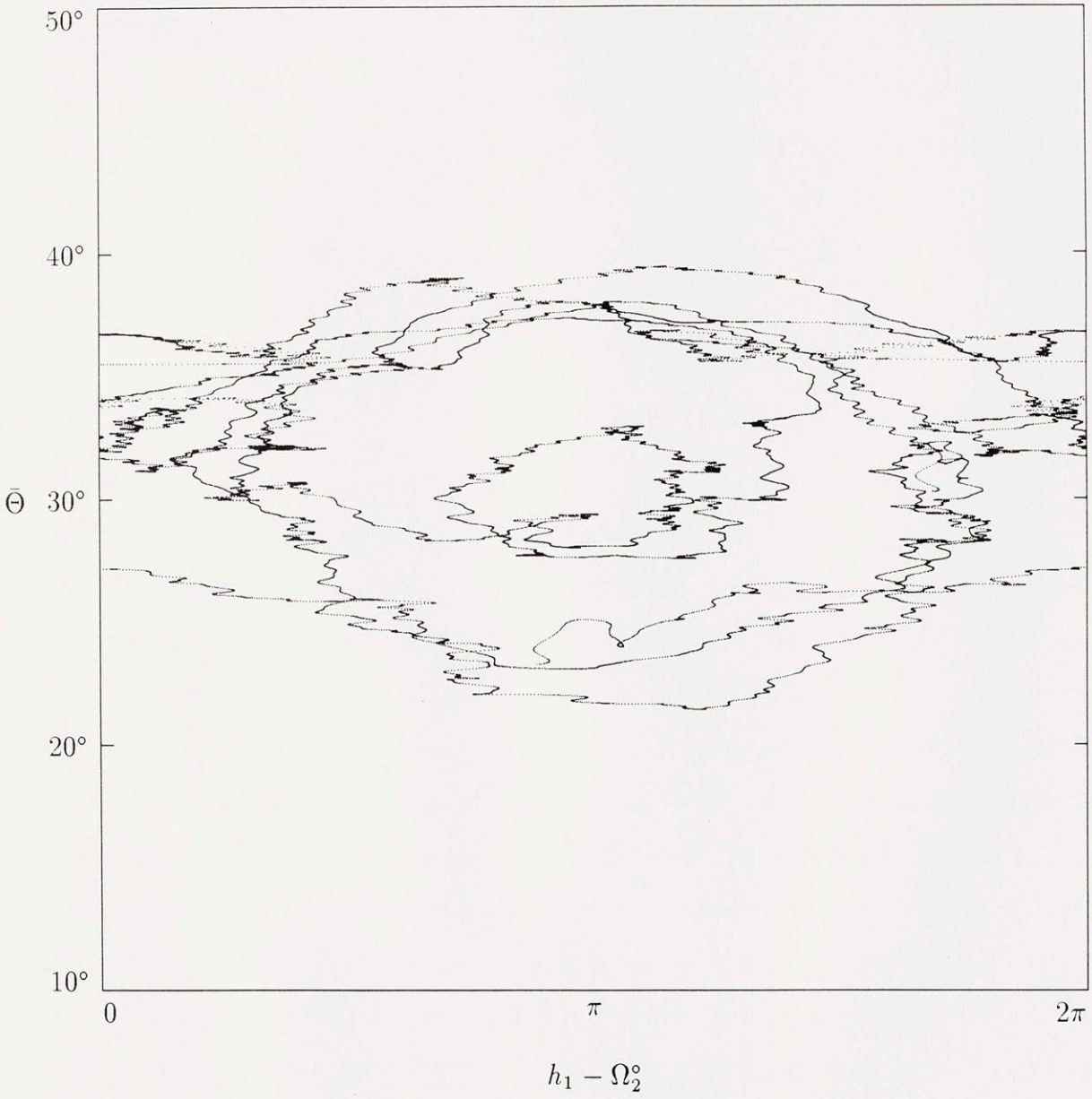

Figure 3-4: The secular spin-orbit resonance is illustrated in this plot of the mean obliquity versus the principal secular spin-orbit resonance angle. For clarity, only the data for the most recent 40 million years are plotted.

obliquity as the resonance is crossed.

It is amusing to note that the large change in mean obliquity about 4 million years ago does not happen in our model if the general relativistic corrections are not included. We have carried out a full direct integration spanning 20 million years without relativistic corrections and did not find large variations in the obliquity. This is perhaps not surprising since general relativity induces changes in the secular mode frequencies, particularly the first two frequencies, that are large compared to the frequency spread of the important multiplet near the second normal mode. Perhaps the geology of Mars will ultimately provide another test of the validity of general relativity.

3.0.4 Adiabatic Chaos

Isolated spectral components in the Fourier decomposition of the orbital variations imply a region of libration of the corresponding non-linear secular spin-orbit resonance. However, in Laskar's Fourier decomposition of the orbit of Mars the resonances corresponding to the components of the multiplet near the second inclination mode are not isolated: the width of the libration zones for the principal components are much larger than the frequency separation of the components.[47] The resonance overlap criterion [10] immediately suggests that the evolution of the obliquity of Mars is chaotic. However, the evolution of the obliquity of Mars is better understood in another way which takes advantage of the small frequency spread of the multiplet. Again, the multiplet of secular spin-orbit resonances can be combined into a single coherent resonance with parameters that vary with a frequency comparable to the frequency splitting of the multiplet. As the resonance parameters vary the size of the libration region can vary drastically, but at the same time the amplitude of the motion adjusts to approximately preserve the resonance adiabatic invariant. Taken together these two facts imply that some trajectories can be forced across the time-varying separatrix. As the separatrix is crossed there is an irregular jump in the value of the adiabatic invariant, determined by the relatively rapidly rotating phase of the resonance variable. Wisdom [49] pointed out that repeated separatrix crossings while

resonance parameters change slowly can give rise to chaotic behavior, and that the size and shape of the chaotic zone can be well approximated by the set of trajectories that are forced to cross the separatrix. This mechanism of "two-timescale chaos" or "adiabatic chaos" was independently discovered by Menyuk [28] and analyzed by Escande [16]. Wisdom was concerned with explaining the large chaotic zones near mean motion resonances in the asteroid belt, and dealt with a coherent resonance representing a multiplet of mean-motion resonances with time evolving parameters governed by the slower secular evolution of the eccentricity and perihelion. Escande dealt with the more abstract problem of a mathematical pendulum with explicit time-varying parameters. The chaotic spin dynamics of Mars is an example of adiabatic chaos, but with an interesting twist. In the spin dynamics of Mars, the time variation of the resonance parameters that drive the spin-system repeatedly across the resonance separatrix are also chaotically varying because of the chaotic evolution of the solar system. However, the evolution of the spin-dynamics of Mars is separately chaotic and does not directly inherit its chaotic character from the chaotic character of the evolution of the solar system. The spin-dynamics of Mars would still be chaotic even if the solar system was quasiperiodic rather than chaotic provided the spectrum of the orbit variations contained sufficiently strong multiplets. We have verified this by computing the evolution of the spin of Mars over 100 million years with the orbit of Mars represented by the most important terms in Laskar's Fourier decomposition. With the assumption of principal axis rotation, the evolution of the spin axis is governed by the simplified time-dependent one degree-of-freedom Hamiltonian

$$\bar{H} = -\frac{\alpha}{2}\left[Z + \frac{\dot{\Omega}(t)\cos[i(t)]}{\alpha}\right]^2 + \dot{\Omega}(t)\sin[i(t)]\sqrt{1-Z^2}\cos(z), \qquad (3.1)$$

where z is the ascending node of the equator plane on the orbit of Mars(simply related to $h_1 - \Omega_2^\circ$) and is the coordinate canonically conjugate to the momentum Z, the cosine of the obliquity of Mars. The precession constant $\alpha = (3\pi/P)(D/P)J_2/\lambda$, where P and D are the orbital and rotational periods of Mars, respectively, has the value $\alpha = 8.26$ arcsec/year for our adopted physical parameters. The orbital precession frequency $\dot{\Omega}$ and the orbital inclination i are simply given as functions of the

quasiperiodic expansion of the orbit(for details see Appendix A). The terms included in the expansion are those used by Ward and Rudy [46]. We find that the evolution of the obliquity in this simplified model is still chaotic with an exponential divergence timescale of about 5 million years, similar to that found in our full numerical integrations, which integrate the rotation of the axisymmetric Mars without approximation and automatically include the chaotic evolution of the solar system.

The mechanism of adiabatic chaos in the spin-dynamics of Mars can be illustrated by considering the simplified model with only the two strongest components of the orbit variation near the secular spin-orbit resonance. The system has a single degree of freedom with periodic forcing at the difference frequency. A stroboscopic surface of section for this model is shown in Fig. 3-5. Points are plotted once per cycle of the periodic forcing. At the chosen phase of the section the coherent combination of the two resonances is at maximum amplitude, and the maximum variation of mean obliquity is represented on the section. We see that only two components are sufficient to give a large region of chaotic behavior in the spin-dynamics of Mars. The range of obliquity variation in the simple model matches rather well the range of mean obliquity observed in Fig. 3-4. The coherent resonance that models the two components varies in amplitude and phase. Trajectories inside the separatrix when the amplitude is maximum are forced to cross the separatrix as the amplitude decreases and the separatrix shrinks. Thus the chaotic zone is nearly identical to the region enclosed by the separatrix at the maximum amplitude. We superposed on the surface of section a solid curve which delimits the predicted chaotic zone at the chosen phase. The size and shape of the chaotic zone are accurately predicted. Keep in mind though that the quasiperiodic representation of the orbit variations is only valid for a few million years, the actual coherent resonance parameters vary chaotically as the orbit varies chaotically.

3.0.5 Parameter Sensitivity

We emphasize that the orbital dynamics is no longer a limiting factor in determining the obliquity of Mars over, say, the last 10 million years. All of the orbit models

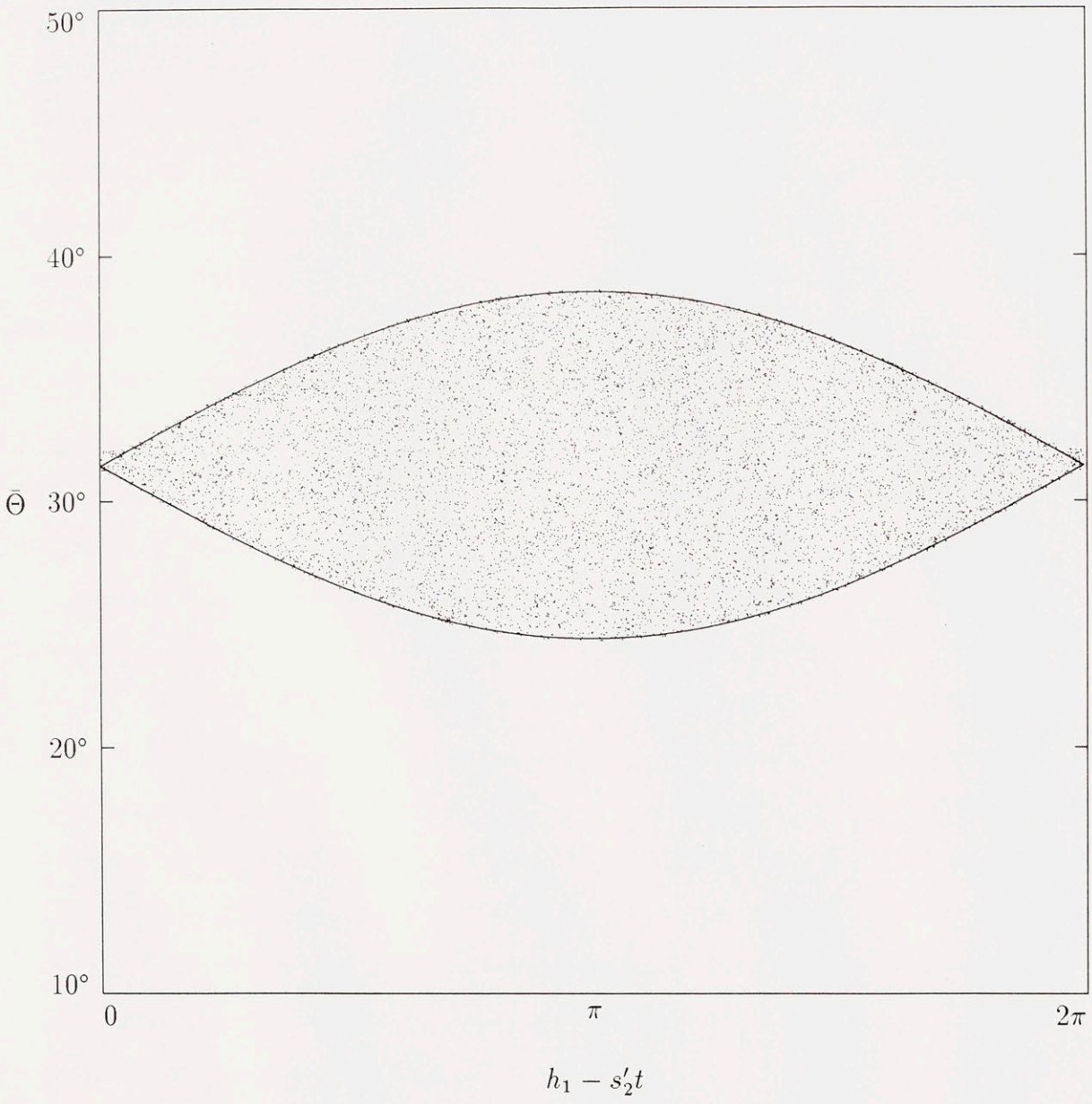

Figure 3-5: A surface of section for the simple two-term quasiperiodic orbit model shows a large chaotic zone that completely engulfs the secular spin orbit resonance. The solid line delimits the predicted region of chaotic behavior in the two resonance model. The agreement is rather good.

give qualitatively the same results, with nearly identical transitions in mean obliquity about 4 million years ago. However, if the physical parameters of Mars were determined to be significantly different from the nominal values we have used, the calculated evolution of the obliquity of Mars could be radically altered. To evaluate the sensitivity to physical parameters we have integrated the quasiperiodic model over a range of physical parameters, keeping the initial conditions of Mars fixed. The crucial parameter is the precession constant; for our adopted physical parameters $\alpha = 8.26$ arcsec/year. We find that in the quasiperiodic model the spin dynamics is chaotic in the range $7.4 < \alpha < 8.6$ arcsec/year. We note that the exponential divergence time for the spin dynamics varied in the range of 1 to 5 million years as α was varied. The range of obliquity also varies with α, with larger mean obliquities associated with larger values of α. Of course, the model is approximate. The full problem should be reexamined if the estimates of the physical parameters are significantly revised.

The history of the obliquity of Mars over longer intervals must be considered to be inherently unpredictable. The evolution of both the orbit and spin of Mars are chaotic and it is inherently impossible to make detailed forecasts of chaotic systems. Also there are the unpredictable long-term changes in the physical parameters of Mars. Thus any calculation of the remote history of the obliquity of Mars could only be considered to be representative of a range of possibilities. These difficulties are only compounded by the possibility that over the age of the solar system the obliquity of Mars may increase secularly as a result of delayed postglacial rebound associated with climate changes induced by obliquity variations.[33] Thus, little constraint can be placed on the primordial obliquity of Mars.

3.0.6 Summary

Our numerical integrations of the rotation of Mars in the field of the fully interacting and chaotically evolving planetary system shows that the spin-dynamics of Mars is chaotic and that the obliquity of Mars undergoes particularly large irregular variations. The large variations in the obliquity are associated with repeated passage

across a secular spin-orbit resonance. The chaotic character of the spin-dynamics is not directly inherited from the chaotic character of the solar system and can be understood to arise through the mechanism of adiabatic chaos. The detailed long term evolution of the obliquity of Mars is inherently unpredictable, but, provided the current estimates of the physical parameters of Mars are not too far from the truth, the obliquity of Mars has almost surely had irregular episodes of high obliquity in the past.

Chapter 4

Conclusion

The dynamics of Mars gave us a hint of the eventful history of planetary rotation. Equipped with the numerical algorithms we described, and a suspicion for complex secular spin-orbit resonances, we can go on and explore the rotational dynamics of other planets and satellites in the solar system. Following a different route, Laskar and Robutel carried out some of these calculations. At about the same time that our results were published [38], they published a study [27] in which they independently confirm the chaotic rotational dynamics of Mars, using Laskar's semi-numerical calculation of a secular solar system. Furthermore, they find that the rotation of the inner planets, excepting the Earth, has large chaotic zones associated with it. They also find that the lunar forcing of the Earth rotation helped the Earth escape the fate of the other planets. They find that the giant planets have regular rotational dynamics, indicating that the obliquities of these planets are very likely to be primordial. Their orbital model does not allow them to investigate the rotation of Pluto.

We believe that a thorough exploration of the rotational dynamics of a planet like Venus, Mercury and most certainly the Earth is constrained by the conservative models used in this paper and those used by Laskar and Robutel [27]. A history of the Earth-Moon system requires the inclusion of the dissipation that results from the tidal distortion of the Earth and the Moon which drastically effects their orbital and rotational evolution. We are currently taking steps in this direction and we will describe the results in a forthcoming report. Furthermore, the rotational dynamics of

the Earth requires us to take account of the coupling between the Earth mantle and core. A Lie-Poisson formulation of the conservative dynamics can be derived from the elegant paper of Poincare [31], giving us a route to the Lie-Poisson algorithm. One can then examine the effect of other forms of coupling including the dissipative torque at a turbulent boundary layer between the mantle and the core. A realistic description of the rotation of Venus must examine the effect of dissipative torques of the Venusian atmosphere or a possible core.

In any case, judging from our first encounters with longterm rotational dynamics in the solar system, it seems just a matter of time before the system yields more of its complex flirtations with resonances and chaos.

Appendix A

Precession: The Slow Road to Chaos

We have explained how the chaotic obliquity of Mars results from the concerted effort of two slow, but resonant dancers dragging a fast one. Such a conspiracy was first written about by Cassini in reference to the rotation state of the Moon. Among other things, Cassini observed that the angular momentum of the Moon remained coplanar with the normal to the ecliptic and the orbital angular momentum suggesting a resonance between the frequencies of precession. Cassini's observations became the subject of theoretical work beginning in the 60s with the papers of Colombo [11] and Peale [29] on this continent, and the work of Beletskii [7] in the former USSR. Here, we intend to go over some of the details we omitted in chap. 3. We will first introduce the slow dancers (the fast dancer, the spin of Mars, does not need much introduction), then go on to examine the dynamics on the celestial dance floor.

A.1 Our First Dancer: The Precession of The Equinox

It is the fate of inclined planetary equators to precess under the action of gravitational torques. Some equators do it faster than others depending on the planets equatorial

bulge, spin rate, inclination, mean motion and the existence of satellites. We discuss the case of an axisymmetric Mars moving on a circular orbit around the Sun. We assume that Mars is in a state of principal axis rotation with angular momentum $M = C\omega$.

The equator precession rate, $\dot{\Omega}_{Eq}$ is much slower than the mean motion and the spin rate of the planet. We can therefore average over these frequencies, and consequently examine the torque that the solar orbital ring exerts on Mars' equatorial bulge. The potential for such interactions is derived by averaging MacCullagh's formula over the mean motion:

$$V_{Body} = -\frac{GM_{Mars}M_{Sun}}{r} + \frac{GM_{Sun}}{r^3}\frac{C-A}{2}(\frac{3}{2}\sin^2\Theta - 1), \tag{A.1}$$

where Θ is the angle between the equator and the orbit plane. The torque acting on the angular momentum conjugate to the generalized angle Θ is equal to minus the derivative of the potential with respect to that angle:

$$T = -\frac{\partial V_{body}}{\partial \Theta} = -\frac{3}{4}\frac{GM_{Sun}(C-A)}{r^3}\sin(2\Theta). \tag{A.2}$$

This torque acts to bring the bulge in alignment with the orbit. In order to recover the precession rate of $\vec{M}$ about the normal $\vec{n}$ to some reference plane, we just divide T by the component of $\vec{M}$ along $\vec{n}$. Let ϕ be the angle between $\vec{M}$ and $\vec{n}$, then the precession rate is given by:

$$\dot{\Omega}_{Eq} = -\frac{3}{4}\frac{n^2}{\omega}\frac{C-A}{C}\frac{\sin(2\Theta)}{\sin(\phi)}, \tag{A.3}$$

or setting $\alpha = \frac{3}{2}\frac{n^2}{\omega}\frac{C-A}{C}$, $\dot{\Omega}_{Eq} = -\frac{\alpha}{2}\frac{\sin(2\Theta)}{\sin(\phi)}$, with $\alpha = 8.26$ arcs/yr currently.

A.2 Our Second Dancer: The Precession of The Nodes

The orbit of Mars precesses in space. The precession frequency is again smaller than the mean motions in the solar system. Following ideas in the previous section, it should be straightforward to get a feel for this behavior. We replace the equatorial

ring with a ring formed by the averaged orbit of a planet and examine its interaction with the ring formed by the averaged orbit of Mars. In case one orbit is inclined with respect to the other a gravitational torque will arise which will tend to bring the orbits into the same plane. This torque causes the precession of the orbits.

The potential energy(up to the second order Legendre polynomial) of the Mars ring in the field of a planetary ring P with $a_{Mars} < a_P$ is given by:

$$V_{Orbit} = \frac{GM_{Mars}M_P}{a_P}\frac{M_{Sun}}{M_{Sun}+M_{Mars}}\frac{a_{Mars}^2}{a_P^2}\left[\frac{3}{8}\sin^2 i - \frac{1}{4}\right], \tag{A.4}$$

where i is the mutual inclination of the orbits. In case, $a_{Mars} > a_P$, the planetary indices should be switched for the approximation to hold. Again the torque experienced by the Mars ring is given by the derivative of the potential energy with respect to i:

$$T = -\frac{\partial V_{Orbit}}{\partial i} = -\frac{GM_{Mars}M_P}{a_P}\frac{M_{Sun}}{M_{Sun}+M_P}\frac{a_{Mars}^2}{a_P^2}\frac{3}{8}\sin(2i). \tag{A.5}$$

Let I be the inclination of Mars' orbit with respect to the reference plane. Then, the precession frequency is given by the torque divided by the component of the ring angular momentum, L_{ring}, along $\vec{n}$:

$$\dot{\Omega}_{Node} = \frac{T}{L_{ring}\sin(I)}. \tag{A.6}$$

Using this formula, we find that the torque exerted by Jupiter causes the orbit of Mars to regress at about 1.97 arcs/yr or with a period of 657 thousand years.

This approach is useful for getting a rough idea of the time scales that are involved. However, the orbits of the planets are eccentric and their dynamics coupled. Faced with this prospect, one has two options. One can look for better and better quasiperiodic approximations of the solar system, a venture started by Laplace-Lagrange and developed to higher orders by Bretagnon [8] and Laskar [23]. However, realizing the chaotic nature of the solar system one develops accurate numerical tools to explore the long term dynamics, an approach taken by Sussman and Wisdom [36]. In our work, we have added another tool in the numerical arsenal. But we have also explored the consequences of a quasiperiodic solar system on the rotation of Mars. So we shall say a few words on the analytic side of things.

The Laplace-Lagrange approximation of the solar system consists of averaging the equations over the fast frequencies, i.e. the mean motion of the planets, and expanding the Hamiltonian up to second order in the eccentricities and inclinations. Having done that, the system becomes linear in the conjugate canonical pairs (p_i, q_i) and (h_i, k_i) where, for small eccentricities and inclinations:

$$\begin{aligned} p_i &= \sin(I_i)\sin(\Omega_i) \quad & q_i &= \sin(I_i)\cos(\Omega_i), \\ h_i &= e_i \sin(\tilde{\omega}_i) & k_i &= e_i \cos(\tilde{\omega}_i). \end{aligned} \tag{A.7}$$

$\tilde{\omega}_i$ is the argument of perihelion, e_i the eccentricity, I_i the inclination, and Ω_i the argument of the node of planet i. The eigenvalue problem is solved and the amplitudes and phases calculated from observations. One can play more complicated versions of this game. Bretagon [8] found a solution which was complete to second order in the masses and third order in the inclinations and eccentricities. Laskar [23] found a solution which was complete to second order in the masses and degree 5 in the inclinations and eccentricities. These solutions lead to a proliferation of frequencies resulting from the coupling between the planets. In the final analysis, the inclination and precession of Mars will be represented by a quasiperiodic series:

$$\begin{aligned} p_{Mars} &= \sum_j N_j \sin(s_j t + \delta_j) \\ q_{Mars} &= \sum_j N_j \cos(s_j t + \delta_j), \end{aligned} \tag{A.8}$$

and

$$\begin{aligned} \dot{\Omega}_{Mars} &= \frac{\dot{p}q - \dot{q}p}{p^2 + q^2} \\ \sin(I_{Mars}) &= \sqrt{p^2 + q^2}. \end{aligned} \tag{A.9}$$

For the problem at hand, we will be interested in those frequencies that are close to the precession frequency of the equator. Table A.2 shows the dominant resonant modes in Laskar's theory as quoted in Ward [47].

A.3 The Couple in Resonance:Cassini States

Here, we assume that the orbit of Mars precesses with a constant rate $\dot{\Omega}$ while keeping a constant inclination i to the ecliptic. We ask: what relationship should exist between i and the obliquity ,Θ, in order for the coplanar configuration, observed by Cassini, to hold? Of course,

$$\dot{\Omega}_{Eq} = \dot{\Omega}_{Node}, \tag{A.10}$$

both precessions being calculated with respect to the ecliptic normal. Using eq. A.3, we get:

$$\frac{\alpha}{2}\frac{\sin[2(\theta+i)]}{\sin(\theta)} = -\dot{\Omega} \tag{A.11}$$

where $\theta = \Theta - i$ is the angle between the equator and reference plane. For $\alpha = 8.26$, $\sin(i) = 0.00131766$ and $\dot{\Omega} = -7.053108 arcs/yr$, the equilibrium condition is satisfied for $\theta_4 = -31.23°$, $\theta_1 = -0.52°$, $\theta_2 = 31.49°$, and $\theta_3 = 179.95$. The strange ordering respects historical convention. A plot of $\dot{\Omega}_{Eq}$ vs θ is shown in Fig. A-1. Depending on values of $\dot{\Omega}$ the problem has two, three or four equilibria. Which of the equilibria are stable and which are unstable? Of course this question could be answered by examining the equations of motion that govern this problem and linearizing around the equilibria. Here, we will address this question using the plot of the precession frequency and physical intuition. Consider a case (Mars' case) where four equilibria exist and let $\vec{n}$, $\vec{e}$ and $\vec{o}$ be unit vectors normal to the reference, equator and orbit planes respectively. We recall that the torque exerted by the Sun on Mars' bulge acts along $\vec{e} \times \vec{o}$.

State 1: In this state, $\vec{e}$ and $\vec{o}$ are on the same side of $\vec{n}$, with $\vec{o}$ between $\vec{n}$ and $\vec{e}$. Increasing $|\theta|$ increases $|\dot{\Omega}_{Eq}|$. $\vec{o}$ lags behind $\vec{e}$. A torque develops which tends to bring $\vec{e}$ closer to $\vec{o}$. This torque contributes an upward kick on $\vec{e}$, thus stabilizing it. The same can be shown for other directions. So state 1 is stable.

State 2: In this state, $\vec{e}$ and $\vec{o}$ are on opposite sides of $\vec{n}$, with both above the ecliptic. Increasing θ decreases $|\dot{\Omega}_{Eq}|$. $\vec{o}$ catches up with $\vec{e}$. A torque develops which contributes an upward kick on $\vec{e}$, thus stabilizing it. So state 2 is also stable.

State 3: In this state, $\vec{e}$ and $\vec{o}$ are on opposite sides of $\vec{n}$, with $\vec{e}$ below the ecliptic,

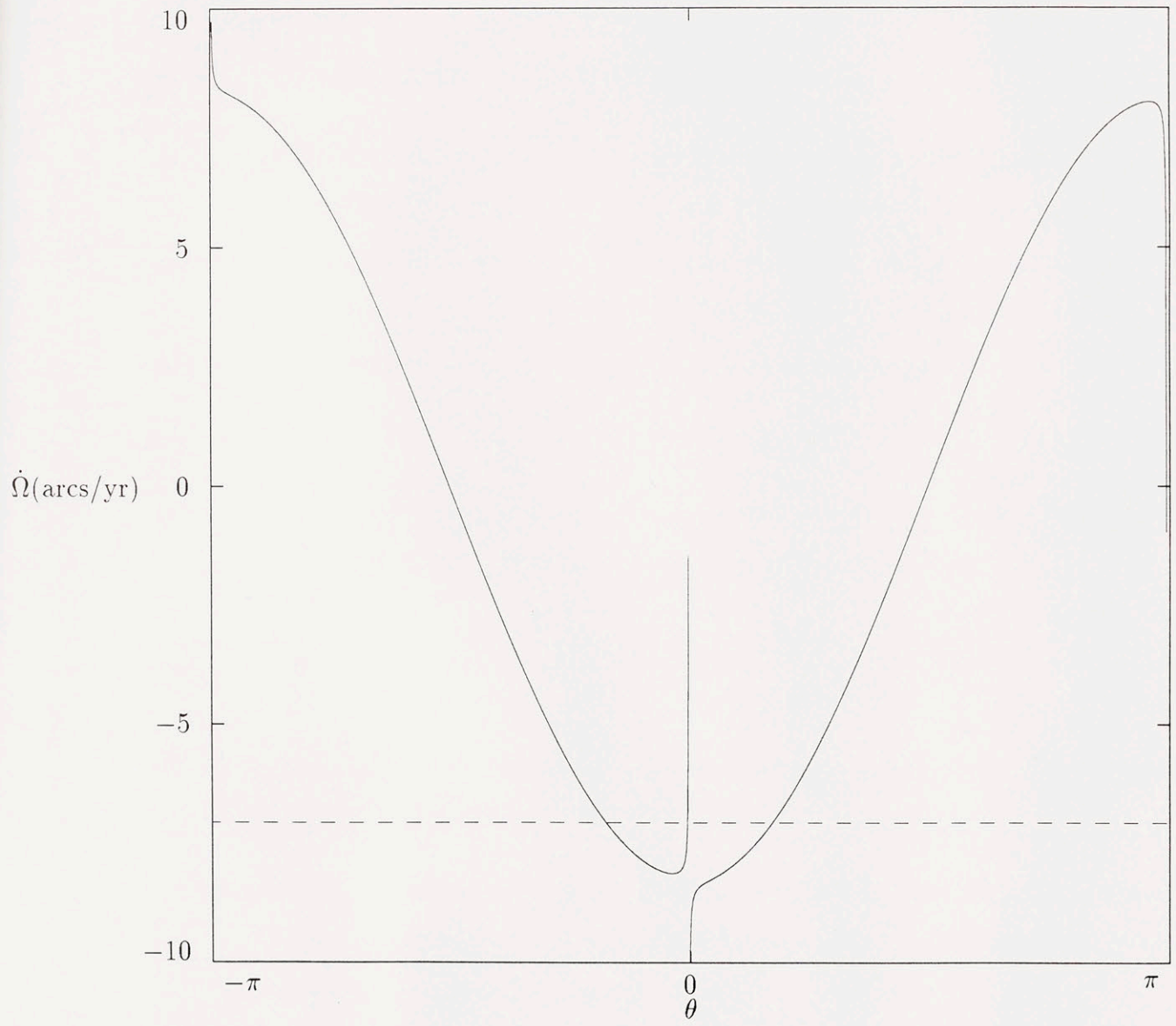

Figure A-1: The solid line shows the change of the precession frequency of the equator with θ. The dashed line is the orbital precession frequency. The points at which the two lines meet are the Cassini equilibria.

closer to $\vec{n}$ than $\vec{o}$ is. Increasing θ increases $|\dot{\Omega}_{Eq}|$. $\vec{e}$ catches up with $\vec{o}$. A torque develops which contributes an upward kick on $\vec{e}$ which stabilizes it. So state 3 is also stable.

State 4: A similar argument shows that state 4 is unstable.

A.4 Dynamics: The Hamiltonian

In order to go past the equilibrium configuration, we need some dynamics and for that we develop the Hamiltonian that governs the problem. We assume that Mars moves on a circular orbit whose inclination and precession are some given functions of time. Let $\vec{\mu}$ be the angular velocity of the orbit in space, and $\vec{\omega}$ be the angular velocity of Mars with respect to the orbit frame. The Lagrangian is:

$$\mathcal{L} = \frac{1}{2}(\vec{\omega} + \vec{\mu}) \cdot \mathbf{I}(\vec{\omega} + \vec{\mu}) - V, \tag{A.12}$$

where $\mathbf{I}$ is the tensor of inertia and V is the potential energy. The angular momentum is equal to $\vec{M} = \frac{\partial \mathcal{L}}{\partial \vec{\omega}} = \mathbf{I}(\vec{\omega} + \vec{\mu})$. The Hamiltonian is then given by:

$$\begin{aligned} \bar{H} &= \vec{M} \cdot \vec{\omega} - \mathcal{L} \\ &= \frac{1}{2}\vec{M} \cdot \mathbf{I}^{-1}\vec{M} - \vec{M} \cdot \vec{\mu} + V. \end{aligned} \tag{A.13}$$

We use MacCullagh's formula for the potential energy. We perform the following operations on the Hamiltonian:

- express the Hamiltonian in terms of Andoyer variables (G, L, H, g, l, h)(referred to the orbit plane) and the semi-major axis a, the inclination $i(t)$ and the precession rate $\dot{\Omega}(t)$ of the orbit;
- average the Hamiltonian over the mean motion;
- enforce the axisymmetry of Mars and average the Hamiltonian over the fast angle g;
- assume principal axis rotation(which is now consistent with the dynamics) and ignore the constant terms in the Hamiltonian.

We end up with:

$$\bar{H} = L\left[-\frac{\alpha}{2}\cos^2(I) - \dot{\Omega}(t)\cos(I)\cos(i(t)) + \dot{\Omega}(t)\sin(i(t))\sin(I)\cos(h))\right]. \quad \text{(A.14)}$$

where $\cos(I) = H/L$ is the obliquity of Mars and α is the usual precession constant. Next we set: $Z = \cos(I)$, $z = h$ and drop the L in the Hamiltonian:

$$\bar{H}_{Mars} = -\frac{\alpha}{2}\left[Z + \frac{\dot{\Omega}\cos(i)}{\alpha}\right]^2 + \dot{\Omega}\sin(i)\sqrt{1-Z^2}\cos(z). \quad \text{(A.15)}$$

The reader can check that (Z, z) is a canonical pair. With this, we complete the derivation of the Hamiltonian for a rigid Mars on a circular orbit with a time dependent orientation.

A.4.1 The Integrable Dance

We examine the dynamics when only one inclination mode is present. Then, $p_{Mars} = N\sin(st+\delta)$ and $q_{Mars} = N\cos(st+\delta)$, $\dot{\Omega} = s$ and $\sin(i) = N$, and the problem is an integrable one degree of freedom problem whose behavior is given by contours of the Hamiltonian. The equations of motion are:

$$\begin{aligned} \frac{dz}{dt} &= -\alpha\left[Z + \frac{\dot{\Omega}\cos(i)}{\alpha}\right] - \frac{Z\dot{\Omega}\sin(i)\cos(z)}{\sqrt{1-Z^2}} \\ \frac{dZ}{dt} &= \dot{\Omega}\sin(i)\sqrt{1-Z^2}\sin(z). \end{aligned} \quad \text{(A.16)}$$

The equilibria are located at $z_0 = 0, \pi$ with Z satisfying:

$$-\alpha\left[Z + \frac{\dot{\Omega}\cos(i)}{\alpha}\right] - \frac{Z\dot{\Omega}\sin(i)\cos(z_0)}{\sqrt{1-Z^2}} = 0. \quad \text{(A.17)}$$

The two conditions can be reduced to Eq. A.11 by setting $I = \theta + i$. Since we have essentially reduced the dynamics to that of a unit vector, it is best followed on a sphere. Fig A-2 shows a projection of the motion for $Z \geq 0$, and $X = \sqrt{1-Z^2}\sin(z)$ and $Y = -\sqrt{1-Z^2}\sin(z)$. We see only three fixed points, the fourth having $Z < 0$. The plane is divided into three regions : Region I consists of counter-clockwise circulation around State 1; Region II is a region of libration around State 2; in region III, the trajectories circulate in a clockwise direction. The regions are separated by two trajectories which are homoclinic to State 4.

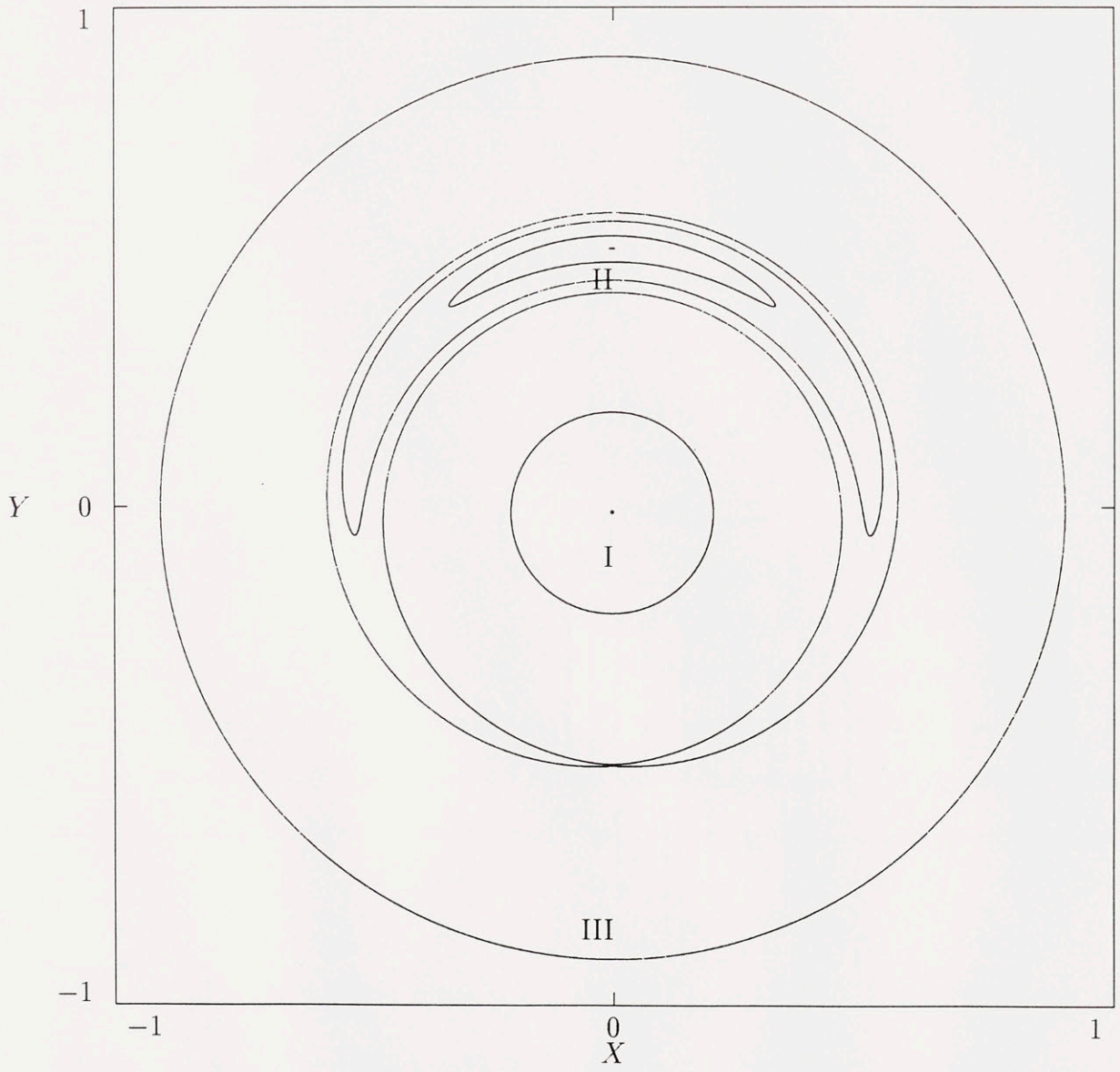

Figure A-2: Contours of of $\bar{H}$ in a case of fixed orbital precession and inclination.

A.4.2 The Two Frequency Dance

We consider a two-frequency secular orbit model which consists of the dominant, near-resonant inclination modes. We have:

$$p_{Mars} = N_1 \sin(s_1\, t + d_1) + N_2 \sin(s_2\, t + d_2)$$

$$q_{Mars} = N_1 \cos(s_1\, t + d_1) + N_2 \cos(s_2\, t + d_2) \tag{A.18}$$

$$\dot{\Omega} = \frac{s_1 N_1^2 + s_2 N_2^2 + N_1 N_2 (s_1 + s_2) \cos[(s_1 - s_2)t + (d_1 - d_2)]}{N_1^2 + N_2^2 + 2N_1 N_2 \cos[(s_1 - s_2)t + (d_1 - d_2)]}$$

$$\sin(i) = \sqrt{N_1^2 + N_2^2 + 2N_1 N_2 \cos[(s_1 - s_2)t + (d_1 - d_2)]}$$

The inclination and precession frequency are periodic with period $T = 2\pi/(s1 - s2)$. The Hamiltonian is a one degree of freedom Hamiltonian with periodic time dependence. $s1$ and $s2$ being very close to each other, we are in a situation of "infinite" resonance overlap in Chirikov's terminology [10]. As i and $\dot{\Omega}$ vary with time, the homoclinic trajectories in Fig. A-2 pulsate. The separatrix extends to maximum width at $t_{max} = -(d_1 - d_2)/(s_1 - s_2)$. As argued in Sec. 3.0.4, the maximum extent of the chaotic zone is well represented by the region bounded by the separatrix at $t = t_{max}$. A planar Poincare section, at maximum separatrix width, was shown in Fig. 3-5, along with the predicted chaotic region . The spherical counterpart is shown in Fig. A-3. The separatrix at maximum width is superposed on the surface of section.

A.4.3 The Quasiperiodic Dance

We examine a quasiperiodic model which incorporates eight of the dominant modes in the inclination of Mars(see table A.2). Here, we lose the benefit of the surface of section, but features of the chaotic adiabatic invariant, associated with repeated separatrix crossings, remain. We examine the past of a trajectory starting with the obliquity of Mars and an azimuth of $3\pi/4$. The 8-frequency model shows a transition to higher obliquity at about 4.5 million years, Fig A-4. The trace of the orbit in the

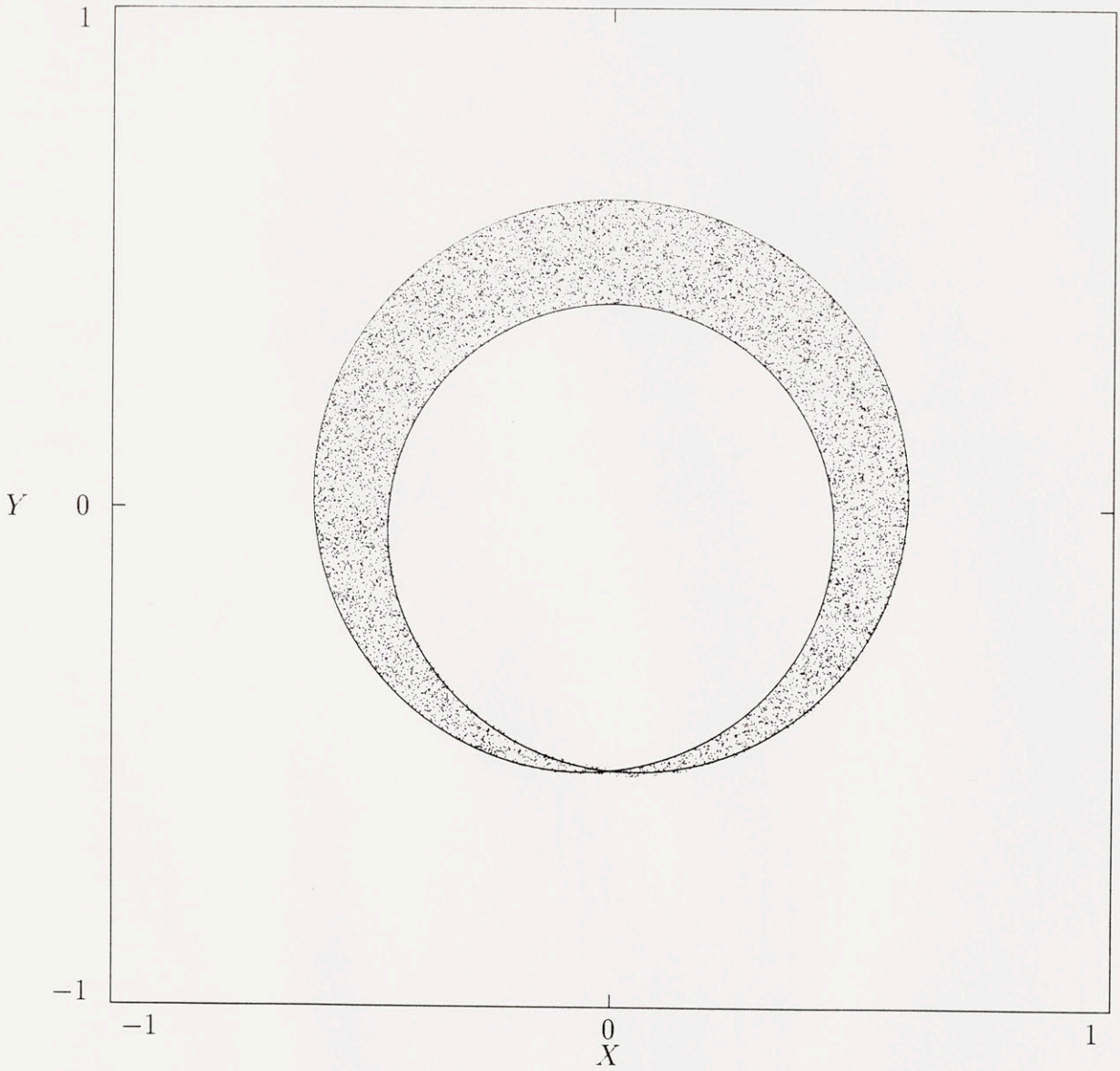

Figure A-3: The separatrix at maximum width is superposed on the chaotic zone of the 2-frequency model. The agreement is rather good.

$X-Y$ plane, Fig A-5 shows the expected transition between libration and circulation. We finally add two high frequency, but large amplitude terms:$s_9 = -17.761481$, $\delta_9 = 286.709047$, $N_9 = 0.071051880$, $s_{10} = 18.744$, $\delta_{10} = 67.263903$, $N_{10} = 0.0237524$. We obtain a trajectory, Fig A-6, which reproduces the qualitative features of the numerical integration. We refer to Laskar [27] for a global picture of the phase space.

A.4.4 The Finale: A Chaotic Dance

The orbital dynamics of Mars is chaotic. The frequencies and phases of the modes vary chaotically in time and quasiperiodic approximations are useful for a very short time in comparison with the age of the solar system. If we add to this the dynamic geology on Mars, we are left with a fundamental obstacle to a reconstruction of the history of the obliquity of Mars. One thing we know for sure is that it is chaotic, and that the present does not represent the primordial conditions.

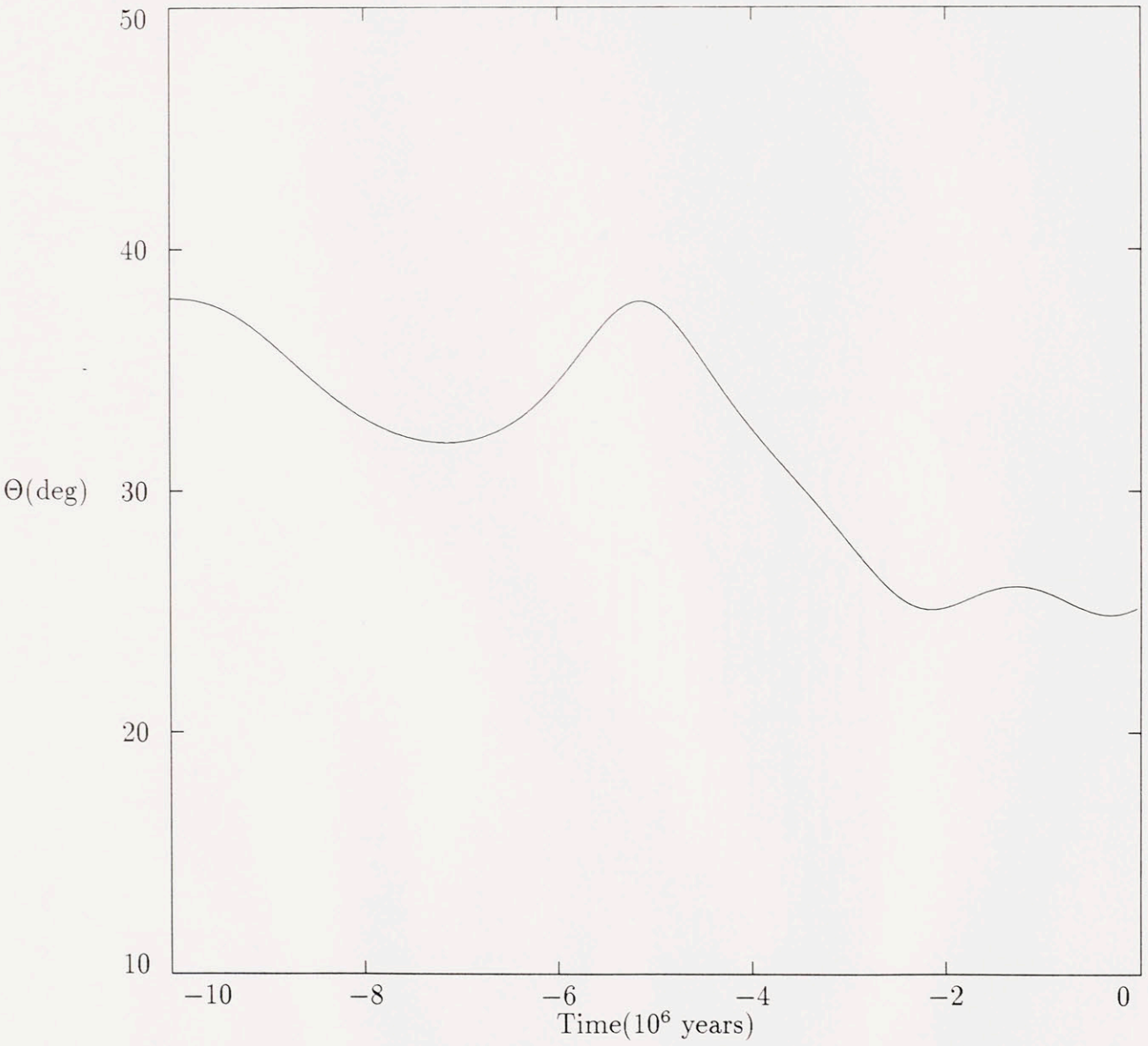

Figure A-4: The past evolution of the obliquity in an 8-frequency model.

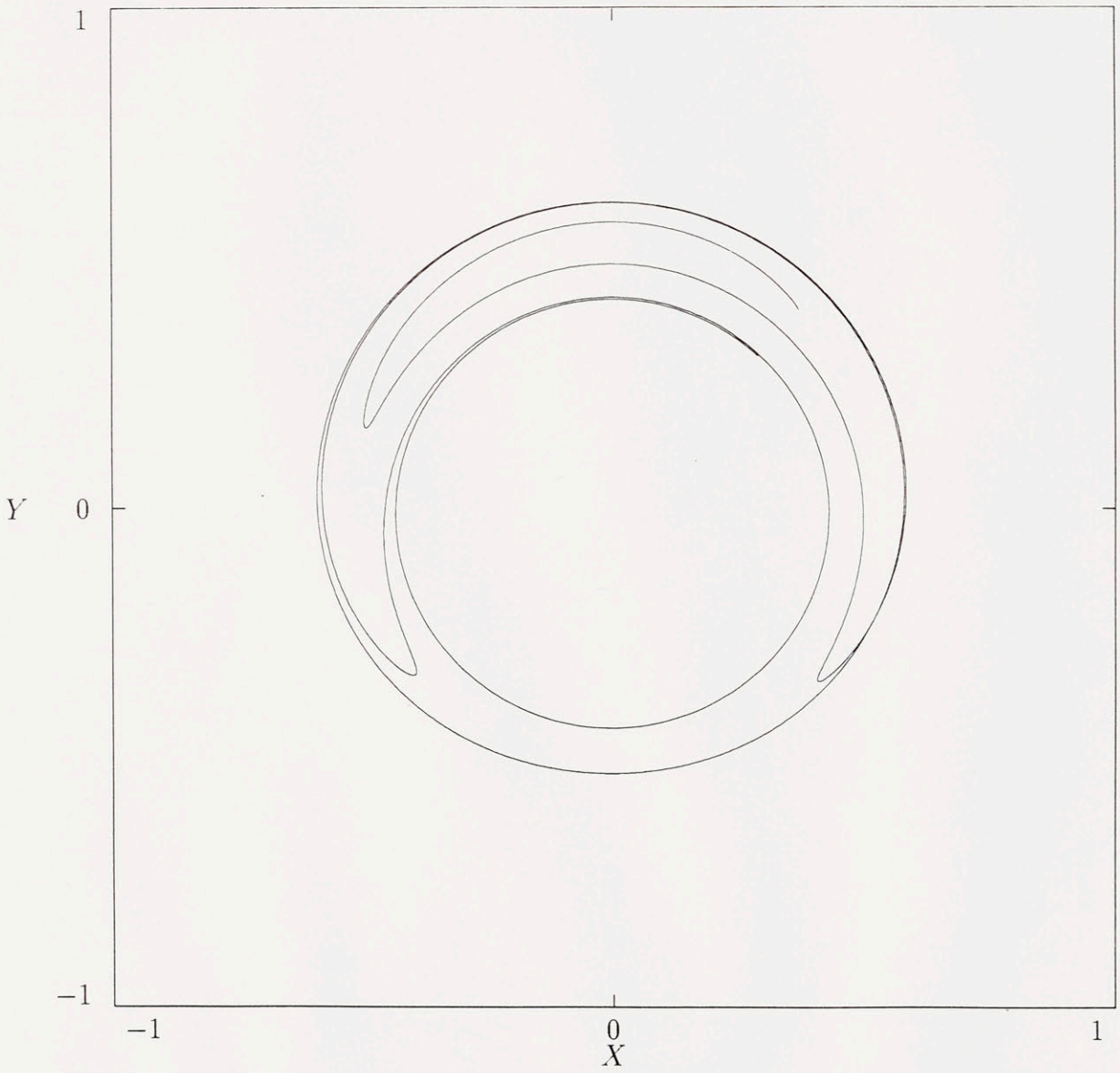

Figure A-5: The same evolution seen in the $X - Y$ plane. Transitions between circulation and libration are evident.

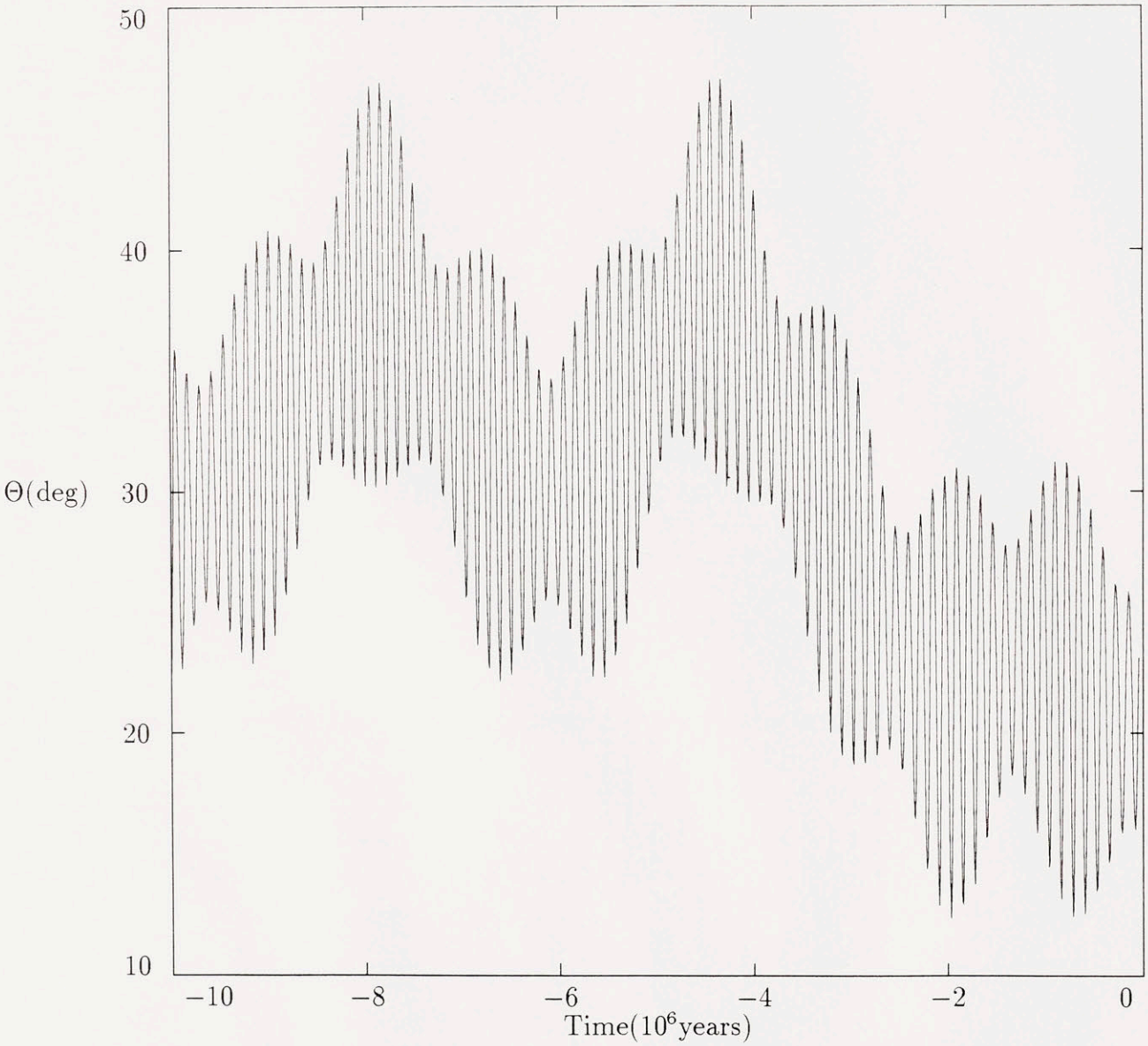

Figure A-6: The past evolution of the obliquity in an 10-frequency model.

s (arcsec/year)	δ (deg)	N
-7.053108	144.957652	0.00131766
-6.963110	311.798757	0.00103666
-7.002513	118.034667	0.00073136
-7.148319	327.622257	0.00068832
-6.860594	298.460307	0.00061120
-7.189558	301.392902	0.000594
-6.813234	330.778441	0.00035216
-6.750999	285.604903	0.00023228

Table A.1: Near-resonant Inclination Modes for Mars' orbit, from Laskar's theory.

Bibliography

[1] H. Abelson, A.A. Berlin, J. Katzenelson, W.H. McAllister, G.J. Rozas, G.J. Sussman, and J. Wisdom, (1992). Preprint.

[2] H. Andoyer, *Cours de Mechanique Celeste, Vol.1*, (Gauthier-Villars, Paris) (1923).

[3] V.I. Arnold, *Ann. Inst. Fourier, Grenoble* **16**, 319 (1966).

[4] V.I. Arnold, *Mathematical Methods of Classical Mechanics*,(Springer-Verlag, New York) (1978).

[5] M.A. Austin, P.S Krishnaprasad, and L.-S. Wang, *SRC Technical Report*, (Systems Research Center, University of Maryland, College Park, MD 20742) (1991).

[6] G. Balmino, B. Moynot, and N. Vales, *J. Geophys. Res.* **87**, 9735 (1982).

[7] V.V. Beletskii, *Celest.Mech.* **6** 356 (1972).

[8] P. Bretagnon, Astron.Astrophys.**30** 141 (1974).

[9] P.J. Channell, and J.C. Scovel, Physica D **50**, 80 (1991).

[10] B.V. Chirikov, *Phys. Rep.* **52**, 263 (1979).

[11] G. Colombo, *Astron.J***71** 891 (1966).

[12] J.M.A. Danby, *Fundamentals of Celestial Mechanics.*, (Willmann-Bell, Richmond) (1988).

[13] M.E. Davies, et al., *Celest. Mech.* **22**, 205 (1980).

[14] M.E. Davies, et al., *Celest. Mech.* **46**, 187 (1989).

[15] A. Deprit, *Am. J. of Physics* **35**, 424 (1967).

[16] D. Escande, in *Plasma Theory and Nonlinear and Turbulent Processes in Physics* (Proc. Intl. Workshop, Kiev, 1987), V.G. Baryakhtar, V.M. Chernousenko, N.S. Erokhin, A.G. Sitenko, and V.E. Zakharov, Eds., (World Scientific, Singapore, 1988).

[17] E. Forest, and R.D. Ruth, Physica D **43**, 105 (1990).

[18] Z. Ge, and J.E. Marsden, *Phys. Lett. A* **133**, 134 (1988).

[19] H. Goldstein, *Classical Mechanics*, 2nd ed.,(Addison-Wesley, Reading, Mass) (1980).

[20] J. Henrard and C. Murigande, *Celest. Mech.* **40**, 345 (1987).

[21] W.M. Kaula, N.H. Sleep, R.J. Phillips sl Geophys. Res. Lett. **16**, 1333 (1989).

[22] W.M. Kaula, *Geophys. Res. Lett.* **6**, 194 (1979).

[23] J. Laskar, *Astron. Astrophys.* **198**, 341 (1988).

[24] J. Laskar, *Nature* **338**, 237 (1989).

[25] J. Laskar, *Icarus* **88**, 266 (1990).

[26] J. Laskar and P. Robutel, *Nature* **361**, 608 (1993).

[27] J. Laskar, F. Joutel and P. Robutel, *Nature* **361**, 615 (1993).

[28] C.R. Menyuk, *Phys.Rev. A* **31**, 3282 (1985).

[29] S.J. Peale, *Astron.J***74** 483 (1963).

[30] S.J. Peale, *Rev.Geo.Space Phys.***11** 767 (1973).

[31] H. Poincare, *Bul. Astron* **27**, 21 (1910).

[32] T.R. Quinn, S.D. Tremaine, and M. Duncan, *Astron. J.* **101**, 2287 (1991).

[33] D.P. Rubicam, *Science* **248**, 720 (1990).

[34] H.C. Plummer, *An Introductory Treatise on Dynamical Astronomy*,(Dover,New York)(1960).

[35] M. Standish, personal communication.

[36] G.J. Sussman and J. Wisdom, *Science* **257**, 56 (1992).

[37] J.R. Touma and J. Wisdom, *Astron.J.*. Submitted.

[38] J.R. Touma and J. Wisdom, *Scinece* **259** 1294 (1993).

[39] O.B. Toon, J.B. Pollack, W. Ward, J.A. Burns, and K. Bilski, *Icarus* **44**, 552 (1980).

[40] L.-S. Wang, , P.S. Krishnaprasad, and J.H. Maddocks, *Celestial Mechanics and Dynamical Astronomy* **50**, 349, (1991).

[41] W.R. Ward, *Science* **181**, 260 (1973).

[42] W.R. Ward, *J. Geophys. Res.* **79**, 3375 (1974).

[43] W.R. Ward, *Astron.J* **80**, 64 (1975).

[44] W.R. Ward, *J. Geophys. Res.* **84**, 237 (1979).

[45] W.R. Ward, J.A. Burns, and O.B. Toon *J. Geophys. Res.* **84**, 243 (1979).

[46] W.R. Ward and D.J. Rudy, *Icarus* **94**, 160 (1991).

[47] W.R. Ward, in *Mars*, H.H. Kiefer, B.M. Jacosky, C.W. Snyder, and M.S. Matthews, Eds., (University of Arizona, Tucson, 1992).

[48] J. Wisdom, S.J. Peale, and F. Mignard, *Icarus* **58**, 137 (1984).

[49] J. Wisdom, *Icarus* **63**, 272 (1985).

[50] J. Wisdom, *Astron.J.***94**, 1350 (1987).

[51] J. Wisdom and M. Holman, *Astron.J.* **102**, 1528 (1991).

[52] J. Wisdom and M. Holman, *Astron.J.* **104**, 2022 (1992).